RSC Advances

REVIEW

View Article Online
View Journal | View Issue

Cite this: *RSC Adv.*, 2025, **15**, 27995

Copper-based nanoparticles for the removal of the crystal violet dye *via* degradation and adsorption: a comparative account

Priyanka Sharma, Supriyo Kar, Mamta Sahu and Mainak Ganguly *

Nanoparticles are almost omnipresent with significant pros and cons. Scientists have ventured into environmental nanotechnology, synthesizing unique nanoparticles in the laboratory. Copper nanoparticles are an active area of research for the decontamination of water from toxic dyes in the context of environmental nanotechnology. Copper is an abundant element in our earth's crust. However, rapid aerial oxidation limits its application. The present review article focuses on removing a toxic dye crystal violet (CV) *via* adsorption and degradation involving copper-based nanoparticles. Various synthetic protocols of such nanoparticles, removal efficiency including reusability, effect of doping and physico-chemical conditions, mechanisms, and connections towards circular economy were summarized here. A comparative account was depicted between adsorption and degradation for the elimination of CV involving copper-based nanoparticles. The current review paper will hopefully be an asset for the industries that release harmful dyes for sustainable water management.

Received 6th June 2025
Accepted 26th July 2025

DOI: 10.1039/d5ra04003e

rsc.li/rsc-advances

1. Motivation

Crystal violet (CV) is a widely used dye in the textile, cosmetic, leather, food, pharmaceutical, paint and varnish, pulp and paper industries. Contaminated waters containing CV are a matter of serious concern. Elimination of dye, employing nanostructured materials involving degradation and adsorption, is an active area of research. Shabna *et al.* illustrated the effect of various factors on the degradation of CV using nanomaterials. Copper is one of the most abundant and biocompatible metals with reasonably low prices. However, susceptibility to aerial oxidation limits its application. By choosing the proper capping agent, copper-based nanoparticles are employed in sustainable water management. Ighalo *et al.*[1] reviewed copper-based nanoparticles for water treatment. However, no review article is available for CV removal *via* a nanometric pathway, including degradation and adsorption, although numerous reports are available on copper-based nanoparticles for CV removal. Such analysis inspired us to prepare this review article.

Solar Energy Conversion and Nanomaterials Laboratory, Department of Chemistry, Manipal University Jaipur, Dehmi Kalan, Jaipur 303007, India. E-mail: mainak.ganguly@jaipur.manipal.edu

Priyanka Sharma

Priyanka Sharma obtained her B.Sc. and M.Sc. degrees from Maharaja Brij University in India. She is now pursuing her Ph.D. degree at Manipal University Jaipur, India, under the guidance of Dr Mainak Ganguly. Her area of interest is material science and environmental science.

Supriyo Kar

Supriyo Kar received his BSc degree from Gobardanga Hindu College under West Bengal State University, India. He was currently completed his MSc degree from Department of Chemistry, at Manipal University Jaipur (India). His area of interest are Nanotechnology and environmental remediation.

2. Introduction

There is a developing freshwater issue worldwide because of the significant effects of industrialization, climate change, and the world's population growth. Therefore, a variety of freshwater consumers and polluters contribute significantly to the depletion of freshwater supplies. These dyes, which come from the textile, cosmetic, leather, food, pharmaceutical, paint and varnish, pulp and paper, and other sectors, include methylene blue, rhodamine B, methyl orange, Congo red, Disperse Violet, methyl red, and CV.[2] According to recent estimates, the globe produces about 70 lakh tons of dyes a year. The environment and human health are seriously endangered when these industrial dye wastes are released into water systems.[3] As evidenced by the significant increase in recent years, this problem has sparked a boom in research. Aquatic ecosystems' photosynthetic activity is harmed when untreated dye-laden wastewater is dumped directly into natural water bodies.[4] Because it contains metals and aromatic chemicals, it can potentially have mutagenic or teratogenic effects on fish species and aquatic organisms. Furthermore, environmental dyes can cause a variety of harmful health effects in humans, such as dermatitis, renal illness, allergic reactions, mutagenicity, and cancer. Particularly complicated in structure and known to have carcinogenic consequences are colors based on chromium.[5] Consequently, the release of dyes into the environment causes water bodies to become contaminated, which affects aquatic life, human health, and water quality.[6,7]

Of late, dye removal has been a very important topic of research for human welfare. Dye removal can be done by two nanometric pathways, one is degradation and adsorption.[8] This study focused on degradation and adsorption pathways.[9] The adsorption path was faster than degradation and was reusable many times, but degradation was about breaking larger hazardous molecules into smaller nontoxic components photocatalytically. The nanoparticle-induced dye degradation and adsorption method was one of the best ways for removing toxic pollutants.[10,11] Peddada *et al.*[12] used photocatalytic removal for hazardous CV dye. Khan *et al.*[13] demonstrated that in wastewater treatment, photocatalysis has become a particularly effective method for breaking down organic contaminants, including synthetic dyes. The process of photocatalysis uses catalysts, like titanium dioxide (TiO_2), to produce extremely reactive hydroxyl radicals ($OH^{\bullet-}$) when exposed to ultraviolet light.[14] Compared to traditional wastewater treatment methods, this procedure has a number of advantages.[15] First, because photocatalysis produces hydroxyl radicals quickly when exposed to light, it is incredibly effective at breaking down organic contaminants. Secondly, it functions under comparatively moderate circumstances with low pressure and temperature, reducing energy use and operating expenses. Third, photocatalysis ensures environmentally friendly wastewater treatment because it doesn't produce any hazardous byproducts.[16]

Furthermore, photocatalytic processes may be easily scaled and modified to fit different wastewater matrices, which allows them to be used in a variety of industrial and environmental contexts. Because of these intrinsic benefits, photocatalysis is a cutting-edge technique for eliminating synthetic dyes and other organic contaminants from wastewater, providing a long-term and effective remedy for problems with water contamination.[17]

Another important technique was adsorption in the case of dye removal. Adsorption is a simpler procedure and more useful than other methods. Adsorption is a well-established technique for removing dyes from wastewater.[18] The procedure becomes even more cost-effective when adsorbents made from other biomass wastes are developed to replace commercial activated carbons. Additionally, recent research has shown that surface chemistry modification may improve the performance of adsorbents.[19] Such modification can be accomplished by adding ionic polymer groups to the adsorbent precursors and by treating them with chemicals, particularly acids and bases. It has been found that adsorbents created exclusively through surface chemical modification function satisfactorily in terms of removing dyes from wastewater.[20] Given their economic

Mamta Sahu

Mamta Sahu received her BSc degree from S.S. Jain Subodh Girls P.G. College (Jaipur, India) and MSc from R. K. Vigyan Mahavidyalya (Jaipur, India). She is currently pursuing her PhD degree under the supervision of Dr Mainak Ganguly in the Department of Chemistry at Manipal University Jaipur (India). Her area of research is environmental nanoscience and spectroscopy.

Mainak Ganguly

Dr Mainak Ganguly received his Ph.D. from the Indian Institute of Technology, Kharagpur, India in 2014. He had acted as a post-doctoral researcher up to 2019 in Furman University (USA) and McGill University (Canada). He is currently working as an Associate Professor in the Department of Chemistry, Manipal University Jaipur (India). His research interests include nanoparticles, clusters, biophysical chemistry, environmental remediations, etc. He has published more than 75 papers and two book chapters.

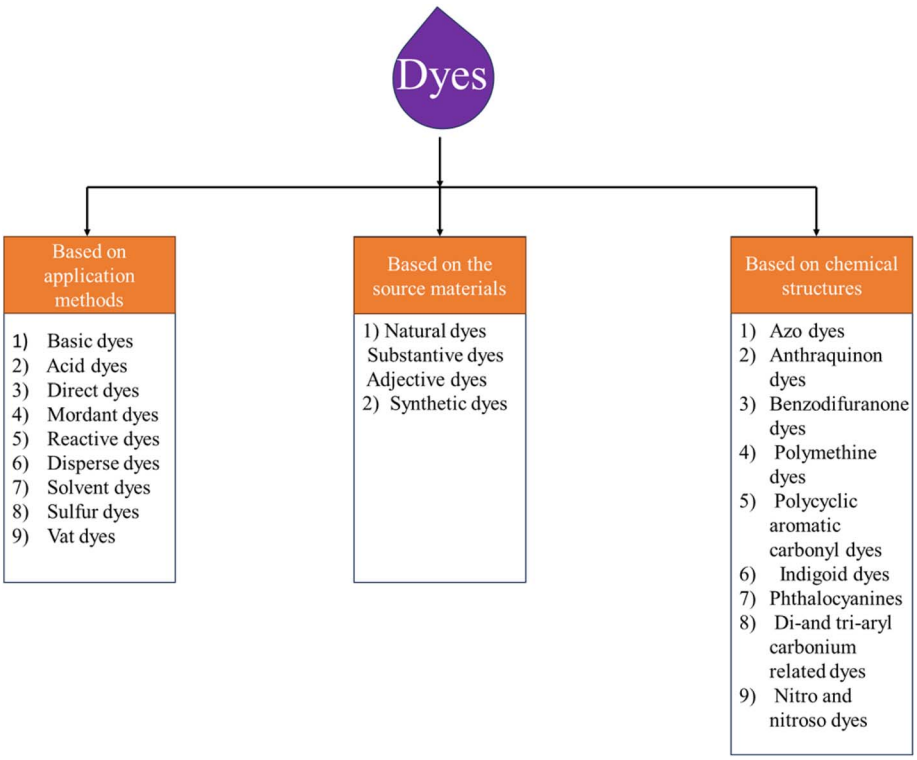

Fig. 1 Flow chart of the different type of dyes.

benefit of requiring less energy during the synthesis process than activated carbon preparations, which need carbonization and activation stages, these findings make modified biomass an appealing alternative for an adsorbent.[21]

In this review study, we focused on using copper nanoparticles to remove dangerous CV dye through adsorption and degradation using logical processes. We discussed the mechanistic aspects and choice of dye, choice of metal surface, synthetic protocol for photo-nanocatalyst and nano adsorbent, limitations, and challenges of the experimental protocol.

3. Choice of dye

Dyes are classified as cationic, anionic, or non-ionic based on their ability to dissolve particle charge in solution. Dye can be classified according to its solubility. Soluble dyes include acid, basic, direct, mordant, metal complex, and reactive dyes, whereas insoluble dyes include sulfur, azoic, vat, and dispersion dyes. Dyes are classified according to their source, application technique, and chemical structure.[22] Dyes are classified into two groups based on their source. There are three main sources of natural dyes: minerals, plants, and animals. Natural dyes are often negative. Substantive dyes are chemically attached to fibers and don't require any additional chemicals.[23] Adjective dyes require a mordant to provide colorfast results. Synthetic colors are derived from both organic and inorganic substances. According to Raval *et al.*,[24] these dyes are widely used due to their low cost and ease of usage, as well as their diverse color spectrum. Synthetic dyes fall into three categories: anionic (acid, reactive, and direct dyes), cationic (basic dyes), and non-ionic (disperse dyes). Fig. 1 classifies dyes according to their usage.

Nonetheless, a variety of dyes are widely used in textiles and natural life, including methylene blue, rhodamine B, methyl orange, congo red, amido black 10b, and coumarin.[25,26] Additionally, these hues are toxic and harmful to human health. Coinage metal has been reported to degrade these dyes thus far. Photodegradation of dyes using copper nanoparticles is an active area of research. Methyl red, methyl orange, phenol red, and eosin y were degraded photocatalytically using copper nanoparticles by Raina *et al.*[27] Sarathi *et al.*[28] reviewed the photocatalytic degradation of malachite green *via* metal oxide degradation. Hydrogen peroxide as a cocatalyst nanostructures were found to be employed an various dyes for degradation.[25] Though ample of review articles are available involving copper nanoparticles for the removal of dyes, CV (a highly carcinogenic dye) was not reviewed in the context of copper nanoparticle-induced elimination for environmental remediation.[27,29,30]

CV is a very useful dye in present life.[31–33] In addition to being used as a topical antiseptic, CV, a hexamethyl pararosaniline chloride dye, has been widely employed as an antibacterial, antifungal, and vermicide agent. Additionally, CV is used in the textile industry as a textile dye and to give printing ink and paints a deep violet hue.[34] Unfortunately, after all these various useful applications, CV dye has a hazardous chemical reactivity to human health. It is a highly active mitotic toxin and a heavy carcinogen clastogen.[35] It tends to develop cancer cells and tumors in the human body. Chemical precipitation,[36]

coagulation,[37] biochemical degradation,[38,39] solvent extraction,[40] sonochemical degradation, photocatalytic degradation,[41] micellar enhanced ultrafiltration, electrochemical degradation,[42] ozone oxidation, ion exchange, and adsorption are some of the methods used to get rid of this kind of dye.[43] Contact on CV for long time on eyes with prolonged exposure, and it's also considered a skin irritant. Although CV has a variety of industrial and medical applications, its potential for toxicity, especially with prolonged exposure, has led to concerns about its safety.[44] In certain cases, it has been linked to genotoxicity and is classified as a potential carcinogen, especially in laboratory and industrial area where workers may have frequent contact with the compound.

Aside from its applications in biology, where it's most used in staining techniques like Gram's stain, CV has also been studied for its potential use in treating infections caused by certain types of bacteria or fungi, due to its bacteriostatic properties. However, its use is more common as a diagnostic tool and in research contexts rather than as a therapeutic agent.[45]

Given its various uses, CV is used in a specific context, like its medical or industrial applications. The cornea and conjunctiva are at risk due to the presence of a cationic dye in the product, as such dyes have been known to cause toxicity to mammalian cells.[46] It has the potential to be absorbed through the skin in harmful quantities, leading to skin irritation and digestive issues. In severe instances, it could result in respiratory failure, kidney damage, and permanent blindness. These serious health risks have driven us to conduct research aimed at removing this dye from wastewater.

The cationic dye CV, which is extremely toxic to mammalian cells, can cause severe eye irritation, painful light sensitivity, and permanent corneal and conjunctival damage. However, in extreme cases, it might induce respiratory and renal failure. Triphenylmethane dye is one of the most regularly used dermatologic agents.[47] CV was once used to treat pinworms in humans and domestic animals, both orally and topically. It is beneficial in suppressing fungal proliferation in several conditions; therefore, it was added to chicken feed to reduce fungal growth, thereby exposing the human population directly or indirectly to CV due to its broad therapeutic and commercial use. CV is a toxic chemical that has been banned from use in aquaculture and the food industry due to its negative impact on human health.[48] Despite its low cost, availability, and efficacy, it is widely utilized in certain aspects. Dye manufacturers typically discharge 10–20% of free dyes into wastewater during the dyeing process. However, the use of azo dyes can increase this value by up to 50%.[49] Discharging a considerable amount of dye in wastewater can harm aquatic resources' aesthetics, gas solubility, and clarity. Removing CV from wastewater from many sectors is crucial for protecting human health, soil, and aquatic ecosystems. Several techniques have been used to remove CV from textile effluent, including chemical oxidation, physical precipitation, photolysis, adsorption, electrochemical treatment, advanced oxidation, reverse osmosis, and biodegradation.[50]

4. Choice of copper

One of the most used materials in industry is copper. Because of its low cost, it is very important in all industries, but especially in the electrical sector. Several techniques have been used to produce and analyze copper nanoparticles.[51] The two key elements that prevent the metal cluster from being used and developed in a new generation of nanoelectronics devices are stability and reactivity.[52] The health and nutrition of plants are greatly influenced by copper, an important mineral that is a component of many proteins and enzymes. Because of its remarkable electrical conductivity, favorable catalytic behavior, and surface-enhanced Raman scattering activity, researchers are interested in using copper nanoparticles as an essential component in future nanodevices.[53]

Copper nanoparticles are used as an addition of lubricating oil to minimize wear and friction efficiently or to repair a worn surface because of their exceptional mending properties.[54] To greatly enhance, nano-copper particles are evenly coated on the graphite surface to provide the charge–discharge characteristics, such as coulombic efficiency, cycle characteristics, and high-rate performance as an anode material for lithium-ion batteries.[55] Copper nanoparticles are widely used for dye degradation due to their high surface area. Compared to other nanoparticles, copper nanoparticles were of great interest due to their lower cost, wide availability, and numerous uses in electrical, sensors, inkjets, field emission emitters, catalysis, and other fields.[56] Copper is therefore favored for the synthesis process due to its high conductivity and inexpensive nature. Copper nanoparticles are frequently employed as antibacterial, antioxidant, anticancer, anti-inflammatory, and anti-hepatotoxic compounds. Copper nanoparticles are now utilized in animal feed, particularly in poultry diets, as an alternative feed ingredient.[57,58] Copper nanoparticles have great catalytic and optical activity. Cu is a 3d element, atomic mass (63.546 u), highly available in the Earth's crust, configuration [Ar] $3d^{10}4s^{1}$. Due to a deficiency of Cu, several diseases, including bone defects, anemia, and Menkes disease, can occur.[59,60] Cu nanoparticles can be used for glucose sensing,[61] dopamine sensing, targeted cancer therapy, microbial warfare reagents.[62] Cu nanoparticles have small dimensions with high electrical conductivity.[63] Cu nanoparticles often also have a fluorescence, lubrication property.[64]

Copper distinguishes itself from metals such as silver, gold, and palladium in dye degradation due to its exceptional amalgamation of visual, chemical, economic, and environmental attributes. Copper nanoparticles (and their oxides, Cu_2O/CuO) demonstrate localized surface plasmon resonance (LSPR) when exposed to visible light.[65] This facilitates the effective formation of energetic electron–hole pairs, which trigger redox reactions: photo-excited electrons convert molecular oxygen to superoxide radicals, while holes generate hydroxyl radicals—both of which are extremely reactive species that decompose dye complexes such as crystal violet. Copper oxides are p-type semiconductors characterized by a low band gap (~1.7–2.0 eV), facilitating efficient visible-light absorption and

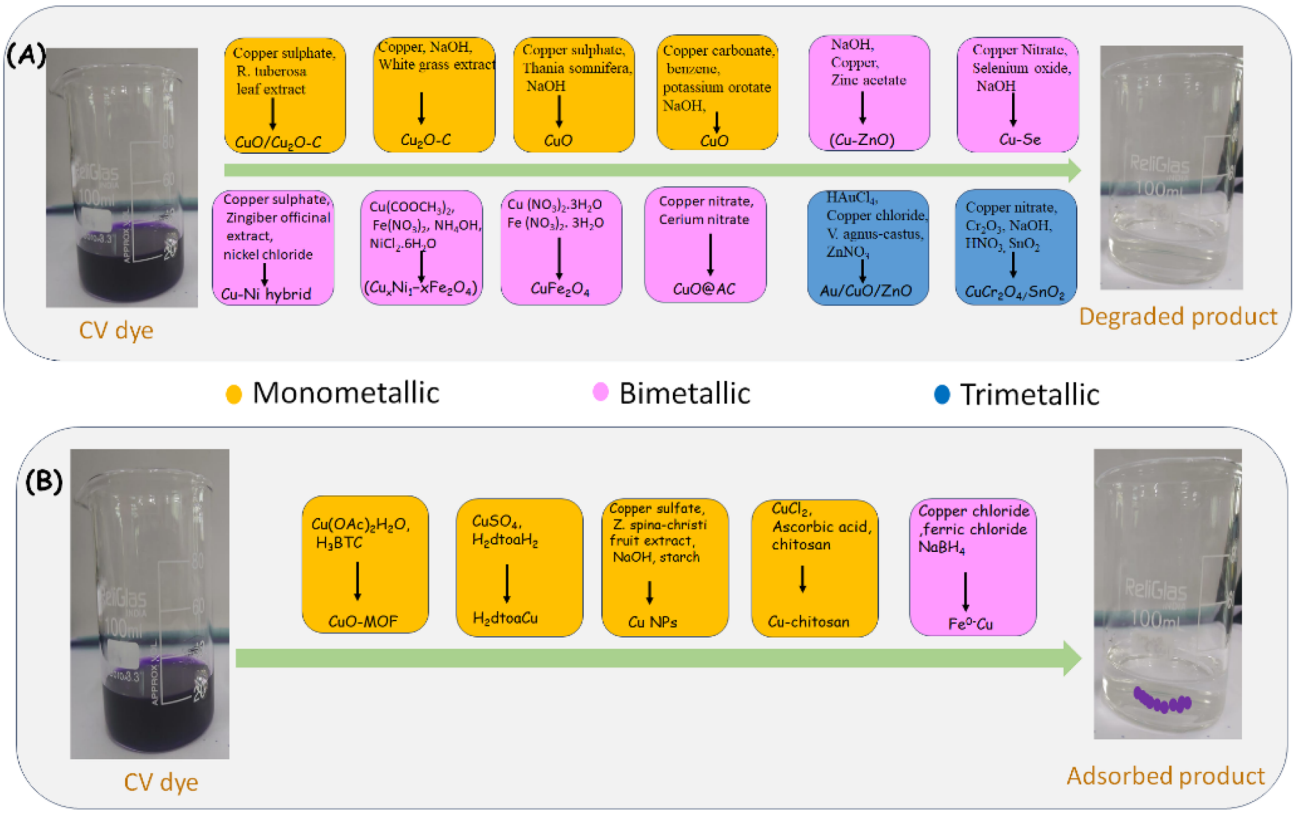

Scheme 1 Schematic representation of the removal of dye with different catalysts *via* (A) degradation and (B) adsorption.

photocatalytic activity.[66] These materials generate reactive oxygen species ($^{\bullet}OH$, O_2^{-}) upon light, facilitating the oxidative degradation of organic dye molecules. In comparison to noble metals, copper has significant economic benefits and superior terrestrial abundance, rendering it appropriate for extensive wastewater treatment. It also endorses green synthesis methods—utilizing plant extracts such as hibiscus or aloe to both decrease and stabilize CuO nanoparticles, resulting in ecologically friendly, biocompatible photocatalysts.

Copper oxide nanoparticles are proficient at generating reactive species and ensuring effective charge separation, and they create heterojunction composites with other semiconductors (*e.g.*, TiO_2, graphene) to further diminish electron–hole recombination. This dramatically boosts degradation rates, at times rivaling or surpassing typical photocatalysts. Noble metals such as silver, gold, and palladium generally exhibit limited redox flexibility and reduced absorption in the visible light spectrum. Silver, gold, and palladium nanoparticles exhibited degradation and adsorption properties. Silver,[67,68] gold,[69] and palladium[70] nanoparticles could also degrade CV dyes, like copper-based nanoparticles. However, adsorption of CV has been limited to silver and copper. Copper is a preferable metal as a photocatalyst and adsorbent because of its cost-effectiveness in comparison to above mentioned metals. Low cost of copper is highly beneficial for large-scale industrial use.

They entail significantly more expenses and difficulties in scaling, rendering copper a more sustainable and pragmatic option for pollutant degradation in water.[71] Copper's strong visible-light localized surface plasmon resonance, redox activity, narrow band gap semiconducting properties, cost-effectiveness, scalable green production, and synergistic composite potential render it an exceptional material for dye degradation, exhibiting both high catalytic efficiency and practical applicability.

5. Nanometric elimination of dye

5.1 Degradation

Dyes are organic compounds commonly used in industries for coloring purposes, such as in textiles and clothing.[72,73] They are typically classified according to the charge they generate when dissolved in an aqueous medium.[74,75] Dyes are mainly divided into natural and synthetic types, which are further categorized based on their charge during ionization into anionic, cationic, and non-ionic dyes.[76,77] Dyes are characterized by their complex structures, which make them stable and resistant to degradation. When dyes contaminate water, they can pollute entire water systems and pose significant health risks to all who rely on the water.[78–80] Research on dye toxicity has shown that even at low concentrations, dyes can be harmful to aquatic life due to the release of toxic chemicals through slow degradation processes,[81] like oxidation, hydrolysis,[82] physical interactions, and chemical reactions.[83] Additionally, dyes can block light penetration in water, reducing photosynthesis and severely

Table 1 Synthesis protocol of copper nanomaterials with CV degradation

Precursor	Nanomaterials	Size/shape	Oxidation state of copper	Condition	Kinetics	Quantity of the catalyst	Time of CV degradation	Energy source	pH
Copper nitrate hexahydrate, NaOH, white grass extract[12]	CuO/Cu_2O–C	38.5 nm/spherical	+2 + 1	pH 10, 400 °C, 24 h	Pseudo-first order	50 mg	240 min	Visible light	3.2
Copper sulphate, *Zingiber officinale* extract, nickel chloride[85]	Cu–Ni hybrid	25.12 nm/irregular	+2	pH 5.7500 °C, 2 h	—	20 mg	20 min	UV light	5.7
Copper(II) sulphate pentahydrate, *Withania somnifera*, NaOH[86]	Cu_2O	410.1 nm	—	80 °C, 2–3 h	Pseudo-first order	50 mg	60 min	Sunlight	—
$HAuCl_4$, copper chloride, *V. agnus-castus*, $ZnNO_3$ (ref. 87)	Au/CuO/ZnO	20 nm/spherical	—	60 °C, 24 h	—	—	36 min	Sunlight	—
$Cu(COOCH_3)_2$, $Fe(NO_3)_2$, NH_4OH, $NiCl_2 \cdot 6H_2O$[88]	($Cu_xNi_1-_xFe_2O_4$)	26 nm −35 nm/spherical	—	60 °C	First order	10 mg	90 min	Sunlight	—
Cu $(NO_3)_2 \cdot 3H_2O$ Fe $(NO_3)_2 \cdot 3H_2O$[89]	$CuFe_2O_4$	10–20 nm/rod-like shape	+2	Thermally 90 °C	—	20 mg L^{-1}	90 s	Sunlight	—
Copper nitrate, cerium nitrate[90]	CuO@AC	—	—	250 °C, 2 h	Pseudo first order	0.6 g	6 min	Microwave/400 W	—
Copper carbonate, benzene (20 mg), deionized water (4 mL),potassium orotate (20 mg), (1 mL),and NaOH, 1,4-bis[(1*H*-imidazole-1-yl) methyl]methanol[91]	CuO	18.2 nm/spherical	—	120 °C, 72 h	Pseudo first order	0.025 mmol	150 min	Tubelight	3–12
Copper nitrate, selenium oxide, NaOH[92]	Cu–Se	32 nm/granular shape	—	60 °C	—	0.5 g	0–120 min	Visible light	8
Copper nitrate, Cr_2O_3, NaOH, HNO_3,SnO_2 (ref. 93)	$CuCr_2O_4$/SnO_2	—	+2, +3	900 °C, 6 h	Pseudo first order	100 mg	90 min	Sun light	7
NaOH, copper, zinc acetate[94]	(ZnO) ($Zn_1{}_xCu_xO$)	20 nm to 25 nm/spherical	—	pH 8, 300 °C, 3 h	Pseudo first order	0.25 mg	3.5 h	UV vis	8
Copper sulphate, *R. tuberosa* leaf extract[95]	CuO	82.33 nm/rod like shape	—	90 °C, 7 h		10 mg L^{-1}	120 min	Sun light/586 nm	—

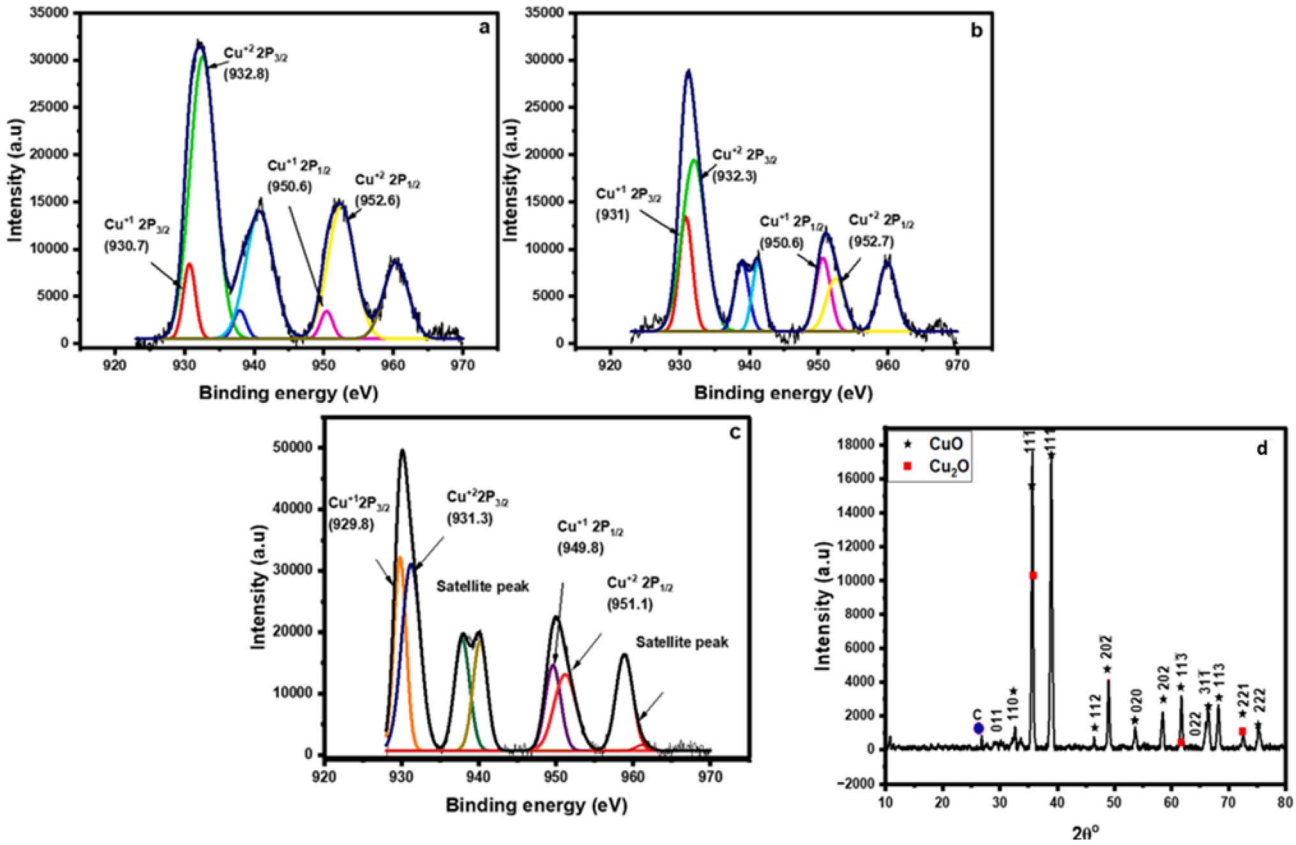

Fig. 2 (a) XPS study of Cu NCs-30, (b) Cu NCs-40, and (c) Cu NCs-50 Cu 2P spectra, (d) XRD spectra of CuNCs.[12]

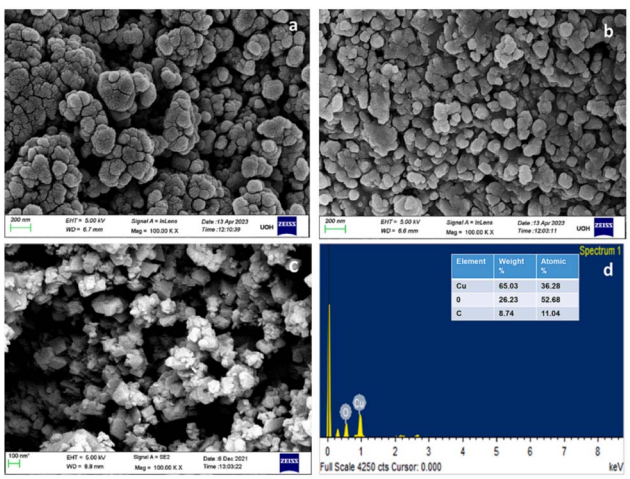

Fig. 3 FE-SEM of Cu NCs synthesized using (a) 30 mL of WGE (b), 40 mL (c), 50 mL (d), and EDAX of Cu NCs-50.[12]

affecting aquatic life. Dyes are also harmful to humans, animals, and aquatic organisms because of their carcinogenic and mutagenic properties.[5] To safeguard human health and other creatures, dyes must be eliminated from water and wastewater from both an environmental and health standpoint. However, treating water contaminated with dyes presents a challenge due to the dyes' resistance to chemical and biological degradation.[84] Researchers have also noticed that dye degradation converts bigger molecules to smaller particles by oxidation or some other chemical reaction. The breaking of the bigger organic pollutants into smaller ones can be done *via* dye degradation (Scheme 1).

As mentioned in Table 1, reports are available for the degradation of CV with copper oxide or metal dopped copper oxide nanoparticles. Though the synthetic protocol involved mostly slightly higher than room temperature (60 °C), $CuCr_2O_4$ nanoparticles were synthesized at elevated temperature (900 °C). The synthesized copper-based nanoparticles were in the size domain 10–410 nm. In other words, nano as well as microparticles were reported to be employed for CV degradation. For the synthesis of such photocatalysts, usually around 2 h of reaction time is needed. However, Somnath *et al.*[91] took 3 days for the synthesis of CuO nanoparticles.

Various synthesis protocols for copper-based nanomaterials used in CV degradation offer specific benefits depending on the precursors and conditions employed. Green synthesis methods using plant extracts, such as wheat grass, *Zingiber officinale*, and *R. tuberosa*, are eco-friendly and cost-effective, enabling nanoparticle formation under mild temperatures. Bimetallic and trimetallic systems, like Cu–Ni and Au/CuO/ZnO, enhanced photocatalytic efficiency through synergistic effects and improved charge separation. Hydrothermal and thermal routes, including those at 80–400 °C, offer better control over particle

size and crystallinity. Microwave-assisted synthesis significantly reduces reaction time while increasing surface reactivity. Ferrite-based nanomaterials like $CuFe_2O_4$ and $CuNiFe_2O_4$ show rapid degradation and magnetic recoverability. Various benefits could be achieved such as reduced synthesis time, lower energy input, enhanced light responsiveness, and improved catalytic stability, contributing to efficient and sustainable dye degradation processes by tuning experimental techniques.

5.1.1 Monometallic

5.1.1.1 Copper oxide. X-Ray diffraction peaks of the CuO/Cu_2O–C heterostructures at 2θ values of 32.6°, 35.7°, 38.9°, 46.3°, 48.9°, 53.6°, 58.4°, 61.7°, 66.3°, 68.2°, 73.2°, and 75.5° corresponded to the (110), (11−1), (111), (112), (20−2), (020), (202), (11−3), (31−1), (113), (221), (222) planes.[96] The XRD analysis indicated that the synthesized Cu NCs were in a mixed crystalline phase of CuO and Cu_2O, with a higher proportion of the CuO phase. A tiny peak at 26.7°, suggesting the (002) plane of carbon particles [Fig. 2]. XPS analysis was used to validate the oxidation status of Cu in the produced Cu NCs. The survey spectrum of the synthesized Cu NCs showed the presence of Cu, C, and O components. The Cu 2p spectra showed two notable peaks: 930.1 eV and 950 eV. The deconvolution of these two peaks revealed copper in two oxidation states: CuO and Cu_2O.[97] Satellite peaks confirmed the existence of CuO in nanoparticles.[98] The shakeup satellite peaks are only visible in substances with the d^9 configuration. The O 1s spectra are deconvoluted into two components at 526.2 eV and 528.3 eV, attributed to Cu_2O and CuO, respectively. The C 1s spectra show five distinct peaks at 282, 283, 286.6, 289.5, and 290.4 eV, corresponding to C–C, C═C, C–O, O–C–O, and O–C═O.[99] The absorption peak at 275 nm signified the existence of CuO nanoparticles, whereas the peak at 395 nm denoted the presence of Cu_2O nanostructures in the produced nanocomposites. Band gaps were calculated to be 1.12–1.53 eV and 1.72–2.05 eV, corresponding to the CuO and Cu_2O phases *via* DRS analysis, demonstrating the presence of both phases.

The morphological features of Cu NCs were investigated using FE-SEM [Fig. 3]. Cu had deformed spherical structures, whereas Cu nanocomposite (NCs) have an uneven polyhedral shape with varying diameters, indicating minor aggregation in the produced Cu NCs.[100] The EDX analysis of the agglomerated Cu NCs-50 revealed Cu (65.03%), O (26.23%), and C (8.74%). The carbon residue from the plant extract might have colonized the interstitial spaces in the produced CuO/Cu_2O NPs, resulted in a CuO/Cu_2O–C nanocomposite.

When exposed to visible light, Cu NCs generated electrons (e^-) and holes (h^+). According to the band gap energy, Cu_2O was an oxidation photocatalyst, whereas CuO is a reducing photocatalyst. Internal electric forces caused e^- and h^+ to split and moved to the particles' external surfaces. Both photogenerated holes and electrons had strong oxidation and reduction capabilities. There was negligible dye degradation (up to 5%) in the blank experiment when C–CuO is used as the photocatalyst, and no degradation without the catalyst, indicating that biofabricated Cu NCs, the nano photocatalyst, are an essential component for the efficient breakdown of CV dye. CuO/Cu_2O–C NCs prepared with 30 mL, 40 mL, and 50 mL of the wheat grass extract were termed as Cu NCs-30, Cu NCs 40, Cu NCs 50. CV solution containing Cu NCs 30, 40, and 50 was photocatalytically degraded under visible light for 240 min. Cu NCs (50) had performed better than Cu NCs (30 and 40). Greater Cu_2O concentration of these NCs allowed for efficient heterojunction formation, resulting in effective degradation. Although Cu NCs-30 and 40 had a small size due to a narrower band gap and difficulty in establishing an appropriate heterojunction due to lower Cu_2O concentration, there might be a greater rate of electron–hole recombination, which hinders the deterioration process.[12]

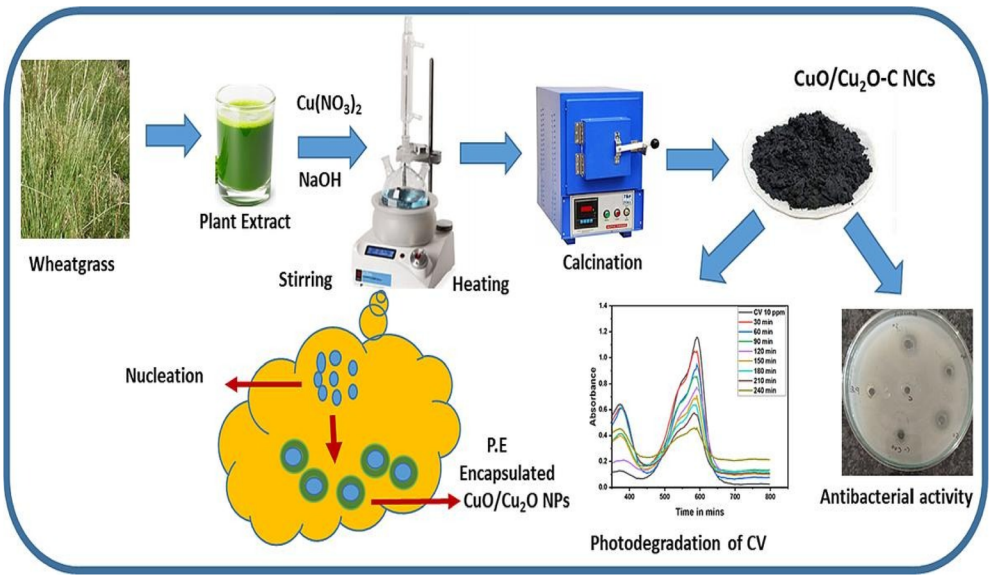

Fig. 4 Schematic representation of copper oxide using wheat grass extract.[12]

In the visible spectrum, CuO is a well-known photocatalyst that is highly effective at photodegrading pollutants without the need of a reducing agent.[101] Copper (CuO/Cu_2O) nanoparticles are widely recognized for their high photocatalytic efficiency in degrading pollutants under visible light, without requiring any reducing agents.[102] However, their industrial application is limited because photogenerated electron–hole pairs recombine quickly. CuO/Cu_2O nanoparticles have great properties on electrical conductivity, magnetic properties and applications, optical and biomedical applications like antimicrobial against Gram positive bacteria.

Peddada *et al.*[12] produced CuO/Cu_2O–C NCs with varied concentrations of white grass extract (WGE) and WGE affects the controlled synthesis of Cu_2O content in nanocomposites (NCs). The CuO/Cu_2O–C nanocomposite effectively destroys CV, a gram stain and pathological effluent, compared to single-phase CuO or Cu_2O. The formation of a heterojunction at the Cu_2O and CuO interface allows for effective charge separation under visible light. The blank experiments were conducted without a photocatalyst and CuO (C–CuO). The results showed no degradation without a catalyst and very little dye degradation (up to 5%) when C–CuO was used as the photocatalyst. The bio-fabricated Cu NCs, the nano photocatalyst, were the essential component needed for the effective breakdown of CV dye. Cu NCs 30, 40, and 50 were added to a 10 ppm CV solution, and photocatalytic degradation was carried out for 240 min under visible light [Fig. 4]. Cu NCs (50), which are made using 50 milliliters of WGE, were found to perform better than Cu NCs 30 and 40. These NCs' greater Cu_2O content allows for effective heterojunction formation, which in turn leads to efficient degradation. However, Cu NCs 30 and 40 may have a higher rate of electron–hole recombination,[103] which slows down the deterioration process, despite their small size due to a narrower band gap and their inability to form a good heterojunction due to a lower Cu_2O content. Increasing the amount of catalysts did not boost the stain solution's breakdown rate as expected. Catalyst buildup can obstruct active areas on the surface, reducing stain adsorption and degradation rates so that it follows pseudo-first-order kinetics mentioned in the below eqn (1).[104]

$$\ln\frac{C_0}{C_t} = k \cdot t \tag{1}$$

The rate constant for degradation, k, was proportional to irradiation time and inversely proportional to dye solution concentration (C_0 and C_t) were the initial and final concentration and time (t) [eqn (1)]. The probability graphs match well with the pseudo-first-order equation, with a regression factor R^2 of 0.9989. After 240 minutes of visible light irradiation with Cu NCs-50, the mineralization percentage of CV was determined using a total organic carbon (TOC) analyzer. To compute the total organic carbon remaining in the CV solution after light irradiation, use the eqn (2) below.

$$\mathrm{TOC} = \mathrm{TOC_f} - \mathrm{TOC_i} \tag{2}$$

TOC_i and TOC_f represent total organic carbon concentrations before and after light irradiation. Irradiation with visible light using CuO/Cu_2O–NCs resulted in mineralization of roughly 50% of the stain into CO_2 and water. The mentioned surface area was 4.626 nm/30.3 $m^2\ g^{-1}$ measured by BET analysis.

Dhara *et al.*[86] demonstrated the photocatalytic activity of biofunctionalized yellow cuprous oxide nanoparticles (Cu_2O NPs) in the degradation of CV. They synthesized Cu_2O NPs using the root extract of *Withania somnifera*, resulting in spherical, monodispersed Cu_2O NPs with an average diameter of 410 nm. In the presence of a reducing agent, sodium borohydrate, and Cu_2O NPs, the photocatalytic degradation of Congo red and CV was employed. The photocatalytic degradation process resulted in a notable reduction of the absorbance maximum at 496 nm due to the breaking of azo bonds. Crystal violet exhibited an absorption maximum at 584 nm, which was significantly reduced by treatment with both $NaBH_4$ and Cu_2O nanoparticles (66.58%) after 60 minutes. The degree of degradation was markedly greater than that of the individual treatments with CV and $NaBH_4$ (49.79%) or Cu_2O NPs (9.63%). The R^2 and K values for the deterioration of CV are 0.869 and 0.015 min^{-1}, respectively.

5.1.1.2 Copper sulfide (CuS). CuS was used to evaluate adsorption tests for CV, rhodamine B, and mixed dyes. The different catalyst dosages (20, 40, 60, 80, and 100 mg) in 50 mL of aqueous dye solution in a dark room.[105] Increasing the catalyst dose from 1.6 mg L^{-1} to 2 mg L^{-1} decreased dye adsorption capability, perhaps due to adsorbent particle aggregation. The degradation efficiency was 56.9% at 1.6 mg L^{-1} and decreased to 45.8% at 2 mg L^{-1} of catalyst. As the concentration of the catalyst increases, the solution becomes more turbid, inhibiting light penetration and activation. The rate constants found are 0.0016, 0.0028, 0.0038, 0.0066, and 0.005 min^{-1} with R^2 values of 0.9899, 0.996, 0.9869, 0.9674, and 0.9859 for 0.4 mg L^{-1}, 1.8 mg L^{-1}, 1.2 mg L^{-1}, 1.6 mg L^{-1}, and 2 mg L^{-1}. The degradation process follows pseudo-first-order kinetics. After centrifugation, an aliquot was obtained every 15 minutes for 75 minutes and analyzed. Equations reflect the equilibrium adsorption capacity (Q_e) and time 't' (Q_t) (eqn (3) and (4)).[106]

$$Q_e = \frac{C_0 - C_e}{W} \tag{3}$$

$$Q_t = \frac{C_0 - C_t}{W} V \tag{4}$$

C_o, C_e, C_t (mg L^{-1}), W, and V represent the initial dye concentration, equilibrium concentration, concentration at a given time, adsorbent weight, and dye volume, respectively. CuS nanoparticles' optical bandgap was determined using the Tauc plot by plotting $(\alpha h\nu)^2$ against $(h\nu)$ and extrapolating the slope of the band edge again. The estimated optical bandgaps are 3.00 eV, 3.26 eV and 3.13 eV for CuS_1, CuS_2 and CuS_3 respectively. The estimated energy bandgaps are greater than that of bulk CuS (1.2 eV).[107,108]

5.1.1.3 Copper with coordinated polymer. Somnath *et al.*[91] demonstrated the synthesis of a novel mixed-ligand hydrogen-

bonded coordination polymer $\{[Cu_2(Or)_2(Bimb)_3]\cdot 4H_2O\}_n$ (KA@CP-S) by hydrothermal methods, utilizing basic copper carbonate in conjunction with 1,4-bis[(1*H*-imidazole-1-yl) methyl]benzene (Bimb) and potassium orotate (OrK) ligands. Topological investigations indicate that KA@CP-S possesses a novel topology characterized by a three-connected uninodal network with point symbol (PS).

KA@CP-S exhibits exceptional photocatalytic degradation and regeneration capabilities, positioning it as a promising and effective future remedial material for the detection and separation of toxic dyes from wastewater contaminated by industrial effluents, which adversely impact algal growth, a crucial and beneficial component of ecosystems. The pseudo-first-order kinetic model was utilized to analyze the photocatalytic degradation of the dye catalyst. After 150 minutes, the peaks nearly disappeared, indicating that coordinated polymer[109] had reached its equilibrium point and decomposed the maximum dye molecules. At equilibrium, mixed-ligand H-bonded coordination polymer $\{[Cu_2(Or)_2(Bimb)_3]\cdot 4H_2O\}_n$ (KA@CP-S) removed a higher percentage of CV (76.1%). The UV-vis absorption spectra show a decrease in dye concentration over time, indicating efficient degradation of the contaminant from aqueous solution. For CV, a significant change in color from violet to clear solution is due to higher photocatalytic degradation of CV dyes. As response time increased with synthesized KA@CP-S, rice husk, and sawdust, CV absorption intensities in water decreased significantly. Absorbance at 590 nm for CV. This displays the statistical histogram for ultimate dye degradation efficacy. The degradation rate of organic dyes catalyzed by synthesized (KA@CP-S) was calculated utilizing.[110]

The absorption intensities of CV dye decreased significantly with increasing illumination time in the presence of KA@CP-S under room. The efficiency of CV degradation was 75.8%. The

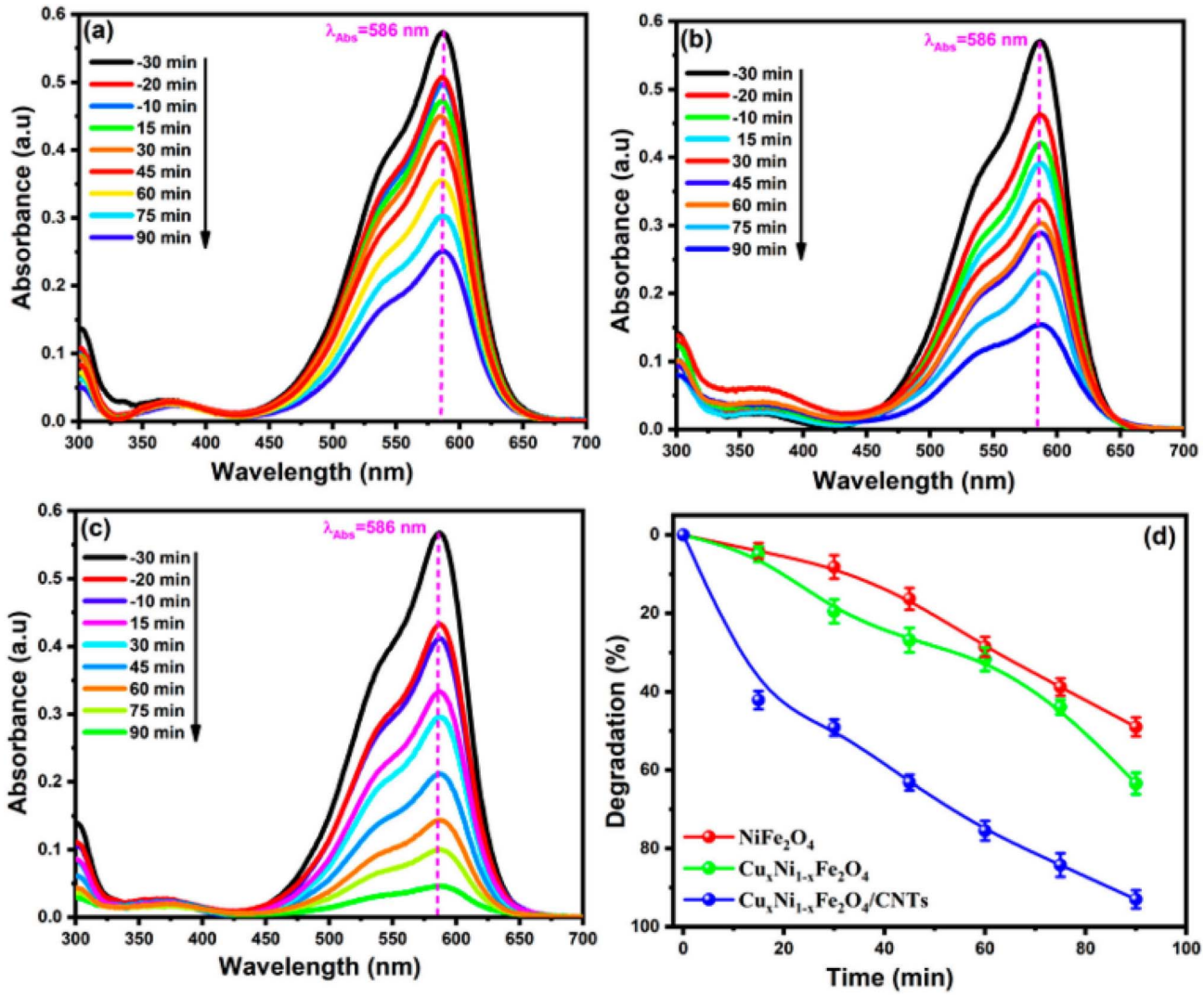

Fig. 5 UV-visible photocatalytic degradation profiles of MB in presence of (a) $NiFe_2O_4$, (b) $Cu_xNi_{1-x}Fe_2O_4$, (c) $Cu_xNi_{1-x}Fe_2O_4$/CNTs, and (d) comparative percentage degradation plots of synthetic photocatalyst.

band gap energy (E_g) was 3.55 eV. The surface area of the bet analysis was 1.84 m^2 g^{-1}.

5.1.2 Copper-doped bimetallic nanocatalyst

5.1.2.1 Synergism effect. The synergistic effect is the combined impact of two or more species, which surpasses the sum of their individual effects. Synergism is a well-known word in the field of catalysis.[111] Metals such as Ag, Cu, Ni, Pd, and Co have a considerable impact on oxygen activation in gold-catalyzed oxidation processes.[112] Unlike the other elements on the periodic table, copper and silver, which belong to the same group (11), usually demonstrate a synergistic effect. Ganguly *et al.*[109] shown the synergistic behavior of gold and silver. This paper focuses on the synergetic activity of copper and cysteine. The strong interaction of cysteine with copper promotes synergistic behavior.

5.1.2.1.1 Cu–Ni hybrid nanoparticles. The most common method for degrading CV dye is to use Cu–Ni hybrid nanoparticles, which are nanocatalysts that excite electrons when exposed to UV radiation.[113] The anticipated benefit of Cu–Ni hybrid nanoparticles is their reduced band gap and ability to absorb a broad spectrum of light, facilitating the generation of holes and electrons for the oxidation of organic dyes. The photonic activity of the Cu–Ni hybrid can be realized under sun illumination. Cu–Ni hybrid nanoparticles (20 mg) were added to 20 ppm of CV dye to study their degradation efficiency. The photo degradation 20 ppm dye solution was exposed to UV-light for 160 minutes after achieving absorption–desorption[114] equilibrium in the dark for half an hour. Degradation was 23% in the first 20 minutes, but increased to 95.6% after further exposure. The rate of dye degradation increased when the irradiation period was extended. The untreated sample of CV dye exhibited no substantial deterioration. The sample showed no substantial degradation when stored in the dark. However, degradation occurs when exposed to light.[85]

5.1.2.1.2 $NiFe_2O_4$, $Cu_xNi_{1-x}Fe_2O_4$, and $Cu_xNi_{1-x}Fe_2O_4$/CNTs. The photocatalytic efficiency of $NiFe_2O_4$, $Cu_xNi_{1-x}Fe_2O_4$, and $Cu_xNi_{1-x}Fe_2O_4$/carbon nanotube (CNTs) was tested and compared for the degradation of an aqueous CV solution in direct sunlight at a catalytic quantity of 10 mg/50 mL.[88] The heterojunction between nanoparticles and CNTs facilitates expedited passage of photogenerated electrons from the conduction band (CB). The increased surface area of CNTs facilitates charge stability and extends their recombination duration. Moreover, the impregnation of ferrites onto CNTs inhibits the aggregation of these magnetic nanoparticles in an aqueous solution.

After predefined intervals, a part of the dye volume was withdrawn from the mixture and its concentration was assessed using a UV-visible spectrophotometer. Fig. 5(a–c) displays the UV-visible time-dependent degradation patterns of CV in the presence of $NiFe_2O_4$, $Cu_xNi_{1-x}Fe_2O_4$, and $Cu_xNi_{1-x}Fe_2O_4$/CNTs. $Cu_xNi_{1-x}Fe_2O_4$/CNTs had the greatest decrease in peak intensity at 586 nm after 90 minutes of solar light irradiation. $Cu_xNi_{1-x}Fe_2O_4$/CNTs showed higher photodegradation efficiency than $NiFe_2O_4$ and $Cu_xNi_{1-x}Fe_2O_4$. $Ni_1Fe_2O_4$, $Cu_xNi_{1-x}Fe_2O_4$, and $Cu_xNi_{1-x}Fe_2O_4$/CNTs resulted in 48.9%, 63.4%, and 92.9% degradation, respectively. $Cu_xNi_{1-x}Fe_2O_4$/CNTs had the greatest decrease in peak intensity at 586 nm after 90 minutes of solar light irradiation. $Cu_xNi_{1-x}Fe_2O_4$/CNTs showed higher photodegradation efficiency than $Ni_1Fe_2O_4$ and $Cu_xNi_{1-x}Fe_2O_4$. $Ni1Fe_2O_4$, $Cu_xNi_{1-x}Fe_2O_4$, and $Cu_xNi_{1-x}Fe_2O_4$/CNTs resulted in 48.9%, 63.4%, and 92.9% degradation, respectively [Fig. 5]. CNT was also preferred for CV degradation. The enhanced photocatalytic activity (92.9%) of $Cu_xNi_{1-x}Fe_2O_4$/CNTs is attributed to the synergistic effect[115] between Cu^{2+} and CNTs in $CuFe_2O_4$. The inclusion of CNTs creates heterojunctions with $Cu_xNi_{1-x}Fe_2O_4$, enhancing electronic interactions at the interface.[116–118] Additionally, photocatalytic activity is increased by the greater dye adsorption due to the interaction between the aromatic components of the dye and the CNTs. The photo-efficiency of produced photocatalysts was evaluated using the first-order apparent rate constant (k_{app}) equation as follows:[88] The mentioned band gap energy (E_g) was 1.54 eV.

5.1.2.1.3 Copper ferrite ($CuFe_2O_4$) nanoparticles. Chen *et al.*[89] utilized nanoscale copper ferrite as a typical ferrite, utilizing CV as the target chemical to examine the behavior of ferrites in the microwave-induced degradation of CV. Copper ferrite has comparatively low dielectric loss. Simultaneously, microwave radiation induces a more rapid deterioration than traditional heating methods, signifying an essential non-thermal action of microwaves with copper ferrite in the process. Microwave-induced holes may account for the effective deterioration. A minor change in CV concentration was observed in the 90 s in $CuFe_2O_4$ dispersion without microwave radiation. However, when coupled with microwave treatment, the majority of chemical vapor was degraded in approximately 60 seconds, resulting in a decline of about 60% in the total organic carbon (TOC) value from an initial concentration of 14 mg L^{-1}. The degradation of CV using a mixture of copper oxide and ferric oxide exhibits a relatively slow rate (apparent reaction rate constant $k = 0.0015$ s^{-1} for 0–50 s). It indicates that simple mixing does not yield the same effect as copper ferrite. Copper ferrite annealed at 673 K demonstrates greater activity for CV degradation ($k = 0.0033$ s^{-1}), while higher annealing temperatures of 873 K ($k = 0.0057$ s^{-1}) and 1073 K ($k = 0.0052$ s^{-1}) improve this efficiency. Results from LC-MS analysis indicate that the components with m/z values of 372, 358, 344, and 330 correspond to parent CV and mono-, di-, and tri-*N*-demethylated intermediates. The *N*-demethylation process occurs in a stepwise manner, with no significant peaks of further demethylated intermediates detected. However, another peak with a m/z of 371 and a retention time of 7.81 min, which was hypothesized to result from the isomerization of CV. This intermediate a more rapid degradation compared to CV, complicating its detection in aqueous solutions subjected to prolonged irradiation times. This implies that as evidence of microwave-induced selectivity, a different degradation pathway is observed with copper ferrite using a different reactant (NiO_x), which requires further study. Relative to the degradation situation at 30 seconds, the concentrations of all *N*-demethylated intermediates decline during 90 seconds of degradation, indicating that mono-demethylation is the controlling step.

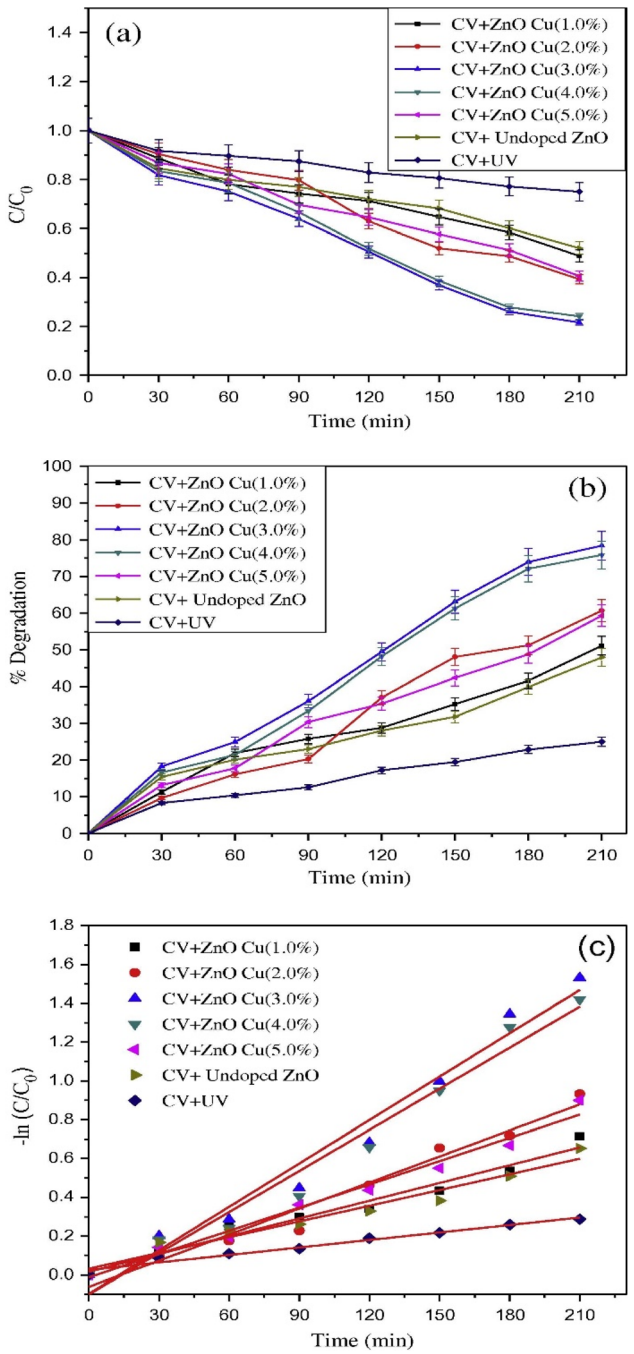

Fig. 6 (a) Photodegradation of crystal violet under varying circumstances (b) degree of disintegration of crystal violet dye across time intervals and (c) kinetics of crystal violet degradation with and without the photocatalyst produced at pH 8.0 under UV-visible light.[94]

5.1.2.1.4 CuO@AC and CeO_2–CuO@AC. Yin *et al.*[90] demonstrated the microwave catalytic oxidation degradation technique for the treatment of CV wastewater without the incorporation of any oxidants. The catalysts CuO@AC and CuO–CeO_2@AC were synthesized by impregnation utilizing activated carbon (AC) as the support, with hydroxyl radicals (˙OH) serving as the oxidants produced during the microwave catalytic process. The approach demonstrated many advantages, including a high degradation rate, brief irradiation duration, and absence of secondary pollutants. This approach shows promise for the elimination of organic pollutants in dye treatment. The degradation rate of CV significantly improved with the addition of a catalyst and increased with the dosage of CuO@AC, likely owing to the enhanced production of ˙OH for the degradation of crystal violet, generated by microwave irradiation on the surfaces of CuO@AC and CuO–CeO_2@AC. A greater catalyst dose results in increased ˙OH generation and enhanced decomposition of CV on the surface of CuO–CeO_2@AC under the same circumstances. CuO–CeO_2@AC has the best removal effectiveness, with a degradation rate of 99.51%. The incorporation of CeO_2 enhances the catalytic activity of CuO@AC. The surface of the doped CeO_2 catalyst exhibits a greater number of active sites and a more uniform dispersion of CuO crystals; CeO_2 acts as a structural additive for the CuO–CeO_2@AC catalyst. The rate constant significantly increased at 400 W, with a linear coefficient of CuO@AC-microwave reaching 0.9927 and rate constants up to 117.92 × 10^{-2} min^{-1}. The degradation of CV in the CuO@AC-microwave system follows a pseudo-first-order kinetic model, and the rate constant for CuO@AC is quite high.

5.1.2.1.5 Copper salenide (Cu–Se). Mahmood *et al.*[92] showed to degrade the CV dye under visible light radiation, an efficient catalyst, copper selenide has been using the chemical precipitation approach. Copper selenide may be utilized to create heterojunction structures such as TiO_2 and WO_3, which possess significant band gaps, to develop novel composite materials with reduced band gaps, hence enhancing the utilization of the solar spectrum for improved photocatalytic efficiency. Polyaniline (PANI) is conductive by nature, it was used to create the synthetic catalytic nano composite, which improved photocatalytic efficiency. The photocatalysis of CV in aqueous solution with varying amounts of the produced composite (0.1–0.9 g). At 590 nm, the production of $O^{2\cdot-}$ and OH˙ radicals cause a consistent decrease in absorbance and an increase in CV decontamination percentage. The optimal catalyst dose for photocatalysis of CV was determined to be 0.5 g. At the optimal catalyst concentration, the produced composite has enough active sites to degrade CV in aqueous solution when exposed to sunlight. Increasing the composite amount beyond the desired value causes catalyst particles to accumulate and reduces the accessible surface area for photocatalyst-reactant contact, leading to worse CV photocatalysis. The influence of time (0–120 min) on CV mineralization in aqueous solution using Cu_3Se_2 at a constant 20 min interval. Extending the time leads to a consistent reduction in absorbance, enhancing the CV's degrading efficiency. The CS-PANI composite exhibits a significant photocatalysis of CV by degrading 56% of CV in 20 minutes and 91% in 80 minutes. As the concentration of dye increases, the number of active sites on the catalyst surface decreases due to excess dye absorption. The excessive dye concentration limits light penetration and photocatalytic interactions, resulting in decreased efficiency degradation. The dye concentration of 40 ppm was determined to be optimal for photocatalysis of CV.

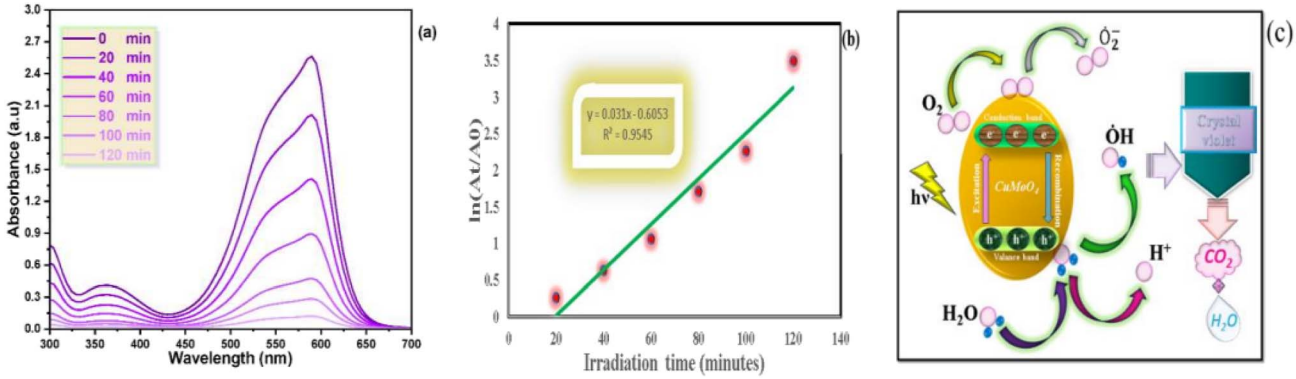

Fig. 7 (a) Decrease in intensity, (b) linear plot and (c) mechanism of dye degradation of $CuMoO_4$ nanostructures.[122]

5.1.2.1.6 Cu doped ZnO nanoparticles. Mittal *et al.*[94] generated nanosized undoped and copper (Cu) doped thioglycerol (TG) capped ZnO nanoparticles (NPs) by a co-precipitation method at different pH levels. The produced nanoparticles used as a catalyst to investigate the photodegradation of CV dye, representing an organic component, under UV-visible irradiation. The intensity of absorption spectra diminishes as the exposure duration extends from 0 to 3.5 hours. The strength of the first peak diminishes owing to the deterioration of the CV dye. The variation in concentration of CV dye as a function of irradiation duration for the dye derivative, both in the absence and presence of undoped and Cu (1.0–5.0%) doped ZnO nanoparticles. The percentage reduction in the concentration of CV dye over time under various settings. Only 25.2% of CV dye dissolved in water is eliminated after 3.5 hours of UV-visible light exposure without the presence of a photocatalyst. The reduced degradation of CV dye may be attributed to the interaction between hydroxyl radicals produced from water and the CV dye. 48.19% of CV dye was destroyed using undoped ZnO nanoparticles. The photocatalytic activity of undoped ZnO nanoparticles arises from defect states induced by donor and acceptor states, including oxygen vacancies, interstitial zinc atoms, zinc vacancies, and interstitial oxygen. Interfacial electron transfer occurs between donor states and the CV dye. They demonstrated degradation rates of 51.5%, 60.7%, 78.7%, 75.7%, and 59.4% of CV dye with Cu (1.0%), Cu (2.0%), Cu (3.0%), Cu (4.0%), and Cu (5.0%) doped ZnO nanoparticles produced at pH 8.0 when subjected to UV-visible light for 3.5 hours. The degradation of CV dye increases from 51.5% to 78.7% at Cu doping concentrations of 1.0% to 3.0%, after which it declines at higher Cu concentrations. This is due to ZnO functioning as a generator of electrons and holes [Fig. 6].

5.1.2.1.7 Cupric molybdate nanostructures. Solar-driven degradation provides a sustainable and economical method for wastewater treatment by harnessing the plentiful and renewable energy of sunlight. It diminishes dependence on artificial illumination or external energy sources, rendering the process more ecologically sustainable and financially feasible.[119] This approach facilitates extensive applications, particularly in areas with elevated solar intensity, and contributes to reducing operational expenses. Moreover, solar radiation may effectively activate photocatalysts, facilitating the degradation of dye molecules without producing detrimental by-products, hence adhering to the principles of green chemistry.[120,121]

Aswin *et al.*[122] reported that the $CuMoO_4$ nanostructures were used for CV degradation under solar radiation, they significantly contribute to the photodegradation of the dye by generating active species. $CuMoO_4$ nanostructures were studied for their photocatalytic activity in aqueous solutions using a photodegradation anionic dye (CV) at 60 ppm. The absorbance intensity maxima and linear CV plots for $CuMoO_4$ nanostructures exposed to solar radiation over time at 550–600 nm [Fig. 7]. $CuMoO_4$ nanostructures in aqueous dye solutions reduced the intensity of deteriorated peaks with increased solar irradiation time. After 120 min of sun exposure, the highest percentage of CV degradation was 96.96%. The Langmuir–Hinshelwood model was used to explain the photodegradation kinetics in the catalyzed process.[123] The band gap energy (E_g) was 2.45 eV.

Adding $CuMoO_4$ nanostructures to a reaction mixture under solar radiation lead to dye photodegradation, resulting in the generation of active species. When sunlight struck the surface of $CuMoO_4$ nanostructures, electrons moved from the VB to the CB, forming electron–hole pairs. Photocatalytic degradation enhanced electron transmission and recombination on $CuMoO_4$ nanostructures. When electron–hole pairs reacted with electron donors (H_2O and hydroxyl ions), the hydroxyl radical was formed. Superoxide radicals were formed during the multi-electron reduction process when one electron became bound with oxygen molecules. The radicals underwent conversion to form hydroxyl radicals. Active species interacted with aqueous dye molecules, producing H_2O, CO_2, and broken-down mineral compounds [Fig. 7].

5.1.3 Copper-doped trimetallic nanocatalyst

5.1.3.1 Au/CuO/ZnO trimetallic nanoparticles. Dobrucka *et al.*[87] demonstrated the biological production of Au/CuO/ZnO trimetallic nanoparticles with *Vitex agnus-castus* extract. Biological techniques use specific benefits of plant extracts, including accessibility, safe manipulation, and diversity of metabolites. Moreover, plant extracts function as reducing and

capping agents in nanoparticle formation and exhibit significant catalytic activity in the presence of dye. Atomic force microscopy investigation revealed nanoparticles ranging from 5 to 25 nm in size. The TEM pictures revealed the existence of locally agglomerated spherical trimetallic nanoparticles. The synthesized Au/CuO/ZnO nanoparticles exhibited significant catalytic efficacy in the reduction of CV. The UV-vis absorption spectra of crystal violet reduction by Au/CuO/ZnO trimetallic nanoparticles synthesized with *V. agnus-castus* extract during 36 minutes. The peak absorbance of CV was observed at 590 nm. After 36 minutes of sunlight exposure, the absorbance intensity peak of CV reduction was shown to decline rapidly and move towards the higher wavelength region.

5.1.3.2 $CuCr_2O_4/SnO_2$ hetero-system. Lahmar *et al.*[93] investigate the physicochemical properties of the spinel $CuCr_2O_4$ and its photoactive effect in the hetero-system $CuCr_2O_4/SnO_2$. This characteristic facilitates the synthesis of the $CuCr_2O_4$ compound and its evaluation as a photocatalyst alongside SnO_2 for the degradation of CV dye under solar light irradiation. The improved photoactivity is ascribed to the transfer of electrons from the $CuCr_2O_4$-CB sensitizer, stimulated by solar radiation, to SnO_2-CB, resulting in the breakdown of organic compounds owing to the prolonged lifespan of charge carriers, which facilitates high mineralization.

The spinel $CuCr_2O_4$ exhibits a direct band gap (E_g) of 1.39 eV, demonstrates stable resistance to photo-corrosion, and generates a cathodic photocurrent indicative of p-type conduction, consistent with the chronoamperometric profile. The flat band potential ($V_{fb} = -0.27$ VSCE) was ascertained through capacitance measurement. At natural pH, the degradation of CV (15 mg L^{-1}) is nearly complete with $CuCr_2O_4/SnO_2$ under sunlight after 90 minutes. The degradation follows pseudo-first order kinetics with an apparent constant 0.012 min^{-1}.

5.1.4 Reusability for degradation. The reusability of nanoparticles in dye degradation is a crucial parameter that directly influences the environmental and economic viability of wastewater treatment processes.[124] Efficient reuse not only reduces the overall cost of nanoparticle synthesis but also minimizes the generation of secondary pollutants, aligning with the principles of green chemistry.[125] Reusable nanoparticles demonstrate high structural and catalytic stability, maintaining their degradation efficiency over multiple cycles, which is essential for long-term application.[126] Somnath *et al.*[91] reported that after the catalytic breakdown of CV by KA@CP-S, the material was thoroughly washed with ethanol many times until all dye molecules were removed, dried, and subsequently utilized for photocatalytic analysis. The feasibility of regeneration and reusability of KA@CP-S, after five cycles, the KA@CP-S retained its original catalytic activity with just a tiny decline in CV degradation efficiency. CV degradation efficiency ranged between 75.8% (1st cycle) and 56.4% (5th cycle). The structure of KA@CP-S remained mostly unaltered after five photocatalytic cycles. Accordingly, the recycling experiments revealed that the KA@CP-S was stable and could be used as photocatalysts for CV deterioration for at least five cycles.

Mahmood *et al.*[92] illustrated that under ideal circumstances, the produced catalytic copper selenide composite was recovered and used again for subsequent batches. This was accomplished by rinsing the produced composite with deionized water and ethanol/methanol in a 1 : 1 ratio for the last sixth cycle the degradation efficiency was about 71.4 percent.

Initially, active sites on nanoparticle surfaces may get occluded by adsorbed dye molecules or intermediates, hence reducing catalytic effectiveness over time. Furthermore, recovery processes—such as centrifugation or filtration—may lead to physical loss or structural modifications, including aggregation or fragmentation, which further diminish performance.[127] A further practical concern is to the scalability of laboratory methodologies. While fundamental washing and drying suffice for small-scale studies, industrial applications require continuous or semi-continuous regeneration systems. Inefficient recovery or prolonged downtime between cycles may diminish the benefits of reuse. Moreover, certain nanoparticles, especially when unsupported, may excessively agglomerate or disperse, complicating recovery and compromising reactor design.[128] Industrial wastewater often contains complex mixtures of dyes, salts, and organic waste. These variables can unpredictably affect the stability or regenerative effectiveness of nanoparticles. Laboratory results are frequently obtained under ideal conditions; nevertheless, performance may decline in real effluents. Pilot-scale testing is essential to determine if nanoparticles will retain their stability and efficacy throughout extended operation.[129] In conclusion, whereas the reutilization of nanoparticles offers notable environmental and economic advantages—such as reduced waste, improved cost-efficiency, and compliance with green chemistry principles—it still faces limitations. Declining efficiency due to fouling and structural deterioration, challenges in large-scale recovery, problems with unsupported particle treatment, and uncertainty in complex waste streams require precise technological solutions and extensive pilot testing.[130]

5.1.5 Mechanism of degradation. The degradation mechanism in dye removal refers to the chemical and physical processes through which dyes are broken down into less harmful or colorless compounds, typically involving photocatalysis, redox reactions, or adsorption.[27] In nanoparticle-assisted degradation, reactive species like hydroxyl radicals or superoxide ions are generated often under light irradiation which attack the dye molecules, breaking their complex structures into simpler, non-toxic substances such as water, carbon dioxide, or small organic acids.[131–133]

CuO/Cu_2O–C heterostructures exhibit photocatalytic activity when exposed to visible light. When exposed to visible light, many holes and electrons are created. The charge transfer process in CuO/Cu_2O–C heterostructures was investigated by determining CB and VB values for each semiconductor. The calculated edge potential for the VB of CuO and Cu_2O is 2.055 eV. CuO and Cu_2O have CB edge potential values of 0.525 eV and −0.208 eV, respectively. Cu NCs create a heterojunction, transferring electrons from Cu_2O's lower potential to CuO's higher potential. Similarly, holes move from CuO's higher potential to Cu_2O's lower potential.[12]

Cu–Ni hybrid NPs are used as a catalyst for CV dye degradation. When exposed to UV light, the NPs excite electrons. The

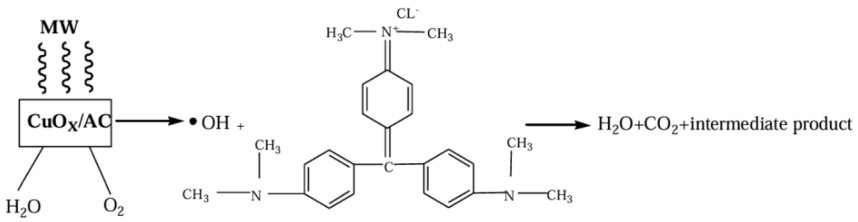

Fig. 8 Reaction route of crystal violet by the MCOD technique with CuO@AC.[90]

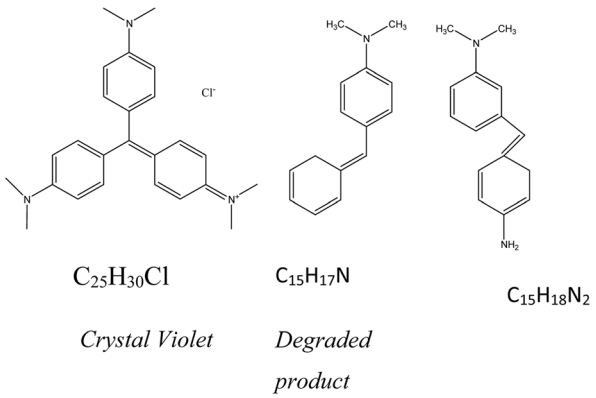

Fig. 9 Theoretical physicochemical properties of before and after degraded dye products.[137]

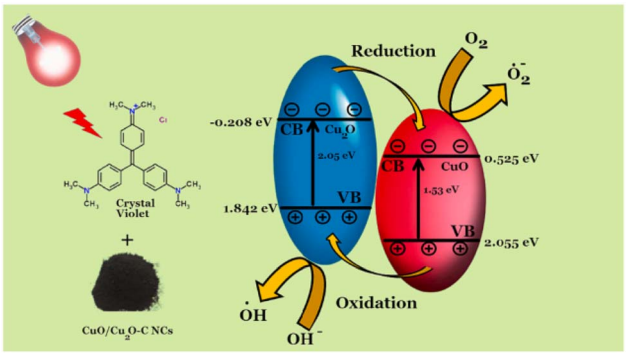

Fig. 10 Mechanism of degradation between CV and copper nanoparticles.

transition from the valence band (VB) to the conduction band (CB) involves leaving a positively charged hole (h^+) in the VB.[134] That hole (h^+) oxidizes CV dye molecules to reactive intermediates due to its high concentration. Hydroxide radicals ($^{\cdot}OH$) are formed when oxidative potential or water molecules react [Fig. 10]. The electron converts molecular oxygen to the superoxide anion radical ($^{\cdot}O_2$). The radicals, in turn were responsible for the breakdown of CV dye.[88]

Microwaves can reduce the electric work function of microwave catalysts in two ways. Microwave irradiation can have a significant impact on dielectric polarization, leading to dipole ordering and a decrease in the electric work function of the catalyst.[135] Microwave energy generates thermal energy, which may be used to heat the catalyst to reduce its electric work function. Microwave electromagnetic waves may directly excite catalysts, resulting in electron–hole pairs (e_{cb}^-–h_{vb}^+), known as the 'photoelectric effect'.[136] Catalysts absorb photons from electromagnetic waves, generating electronics (e_{cb}^-) and electron holes (h_{vb}^+) on the surface of copper oxide@ activated carbon (CuO@AC) and CuO–CeO_2. CuO@AC h_{vb}^+ interacts with absorbed H_2O and OH on the catalyst surface to produce hydroxyl radicals, which are the primary source of $^{\cdot}OH$ production. In e_{cb}^- combines with H_2O_2 and O_2 to generate $^{\cdot}OH$ and superoxide radical anion (O^{2-}).[90]

Solar light excited electrons from $Cu_xNi_{1-x}Fe_2O_4$ CB to higher energy levels, leaving positive holes behind. Cu^{2+} in $Cu_xNi_{1-x}Fe_2O_4$ traps electrons, which were then caught by the highly conductive surface of CNTs.[88] These electrons reacted with oxygen molecules on the photocatalyst surface, producing superoxide radicals. Holes from the CB combined with H_2O molecules to produce hydroxide radicals. The redox process converted primary reactive species (electrons/holes) into secondary reactive species ($^*O^{-2}$/$^*OH^-$). These secondary species attacked the dye molecules (CV), producing CO_2 and H_2O.

$$hv + Cu_xNi_{1-x}Fe_2O_4/CNTs \rightarrow e^- + h^+ \quad (5)$$

$$e^- \rightarrow CNTs(e^-) \quad (6)$$

$$e^- + O_2 \rightarrow {}^{\cdot}O^{-2} \quad (7)$$

$$H_2O + h^+ \rightarrow \cdot OH^- \quad (8)$$

$$\cdot O^{-2} + CV \rightarrow CO_2 + H_2O \quad (9)$$

$$\cdot OH^- + CV \rightarrow CO_2 + H_2O \quad (10)$$

Some studies suggested that oxidants such as H_2O_2, O_2, and ClO_2 could enhance degradation in microwave-assisted procedures for the generation of oxidizing species under microwave irradiation. The quantities of hydroxyl radicals ($^{\cdot}OH$) generated during the microwave catalytic oxidation degradation (MCOD) process utilizing CuO@AC were adequate to promote the breakdown of C, coupled with the probable reaction pathway for this degradation method employing the CuO@AC catalyst [Fig. 8]. No additional H_2O_2 or other oxidants were supplied to augment deterioration in the MCOD process.[90]

The (e^-/h^+) pairs generated on p-$CuCr_2O_4$ when the catalyst was irradiated with an energy superior to E_g, migrated to the

Table 2 Synthesis protocol of copper nanomaterials with CV adsorption

Precursor	Nanomaterials	Size/shape	Oxidation state	Condition of formation	Isotherm/kinetics	Quantity of the catalyst	Time of CV adsorption	Energy source	pH
$Cu(OAc)_2H_2O$, H_3BTC[141]	Cu-metal–organic framework	50 nm	—	—	—	50 mg	7 h	UV/vis	—
Copper chloride dihydrate, ferric chloride hexahydrate, $NaBH_4$ (ref. 142)	Fe^0–Cu	803, 890, and 220.19/irregular (DLS study)	—	pH 7, 110 °C	Langmuir/pseudo first order, pseudo second order	2.0 mg mL^{-1}	15–180 min	UV/vis	3–10
$CuSO_4$, H_2dtoaH_2 (ref. 143)	$H_2dtoaCu$	—	—	60 °C	Langmuir/pseudo first order, pseudo second order	1.2 mg mL^{-1}	100 min	UV/vis	3–12
Copper sulfate, *Z. spina-christi* fruit extract, NaOH, starch[144]	Cu	8–15 nm	—	80 °C	Second order	80 mg	7.5 min	UV/vis	9
$CuCl_2$, ascorbic acid, chitosan[145]	Cu-chitosan	45.6, 63.7 nm/ flowerlike structures	—	70 °C	Langmuir isotherm, Freundlich/second order	149.9 mg L^{-1}	30 min	UV/vis	9.5

opposite poles of the surface, reacted with the adsorbed CV molecules, and gave the electrons to generate intermediate species of $^{\bullet}OH$ free radicals. The electrons reacted with oxygen to form superoxide and hydroperoxide radicals, and hydrogen peroxides, which will then break down into hydroxyl radicals according to the following reactions.[93]

Sanakousar *et al.*[137] demonstrated the influence of cadmium ion doping on the structural, optical, electrochemical impedance, and photocatalytic characteristics of ZnO and Cd–ZnO nanoparticles. Mass spectrometry indicates that CV-dye has entirely deteriorated and fragmented into minor mass signals after 30 minutes ($C_{15}H_{17}N$ and $C_{15}H_{18}N_2$) at pH 10–12. Cd–ZnO compounds may be effectively utilized to decompose cationic dyes [Fig. 9].

The holes reacted with reducers giving rise to strong oxidizing radicals ($^{\bullet}OH$), which were responsible for the oxidation of the CV through the mineralization according to the following reactions[31,137]

$$H_2O + h^+ \rightarrow HO^{\bullet} + H^+ \quad (11)$$

$$OH^- + h^+ \rightarrow HO^{\bullet} \quad (12)$$

$$C_2H_2O_4 + \tfrac{1}{2}O_2 + 2h^+ \rightarrow 4CO_2 + H_2O + 2H^+ \quad (13)$$

$$CV + h^+ \rightarrow CV^{\bullet +} \quad (14)$$

$$HO^{\bullet} + CV^{\bullet +} \rightarrow CO_2 + NO_2 + H_2O \quad (15)$$

5.1.5.1 Critical analysis. The results indicate the efficacy of several copper-based nanomaterials in degrading CV dye, demonstrating notable advancements in photocatalytic applications. CuO/Cu_2O–C nanocomposites produced with wheat grass extract exhibited improved activity owing to efficient heterojunction formation; however, high catalyst loading impaired performance due to aggregation.[12] Biofunctionalized Cu_2O nanoparticles exhibited efficacy in the presence of $NaBH_4$ but demonstrated restricted independent activity, suggesting reliance on co-reagents. CuS nanoparticles had modest efficacy, constrained by dose-dependent factors such as turbidity and particle aggregation. Copper-coordinated polymers demonstrated commendable photocatalytic efficacy and structural innovation; nonetheless, their restricted surface area and scalability may hinder practical use. Bimetallic systems, as Cu–Ni hybrids, demonstrate potential for photodegradation under solar irradiation through bandgap modulation, however their efficacy was limited without prolonged exposure. Cu–Se composites combined with polyaniline exhibited significant degradation efficiency under sunshine; however, elevated dye concentrations diminished efficacy due to site saturation and decreased light penetration. The ternary nanocomposite Cu_x-$Ni_{1-x}Fe_2O_4$/CNTs exhibited enhanced performance due to synergistic charge transfer and adsorption, while intricated production and expense persist as issues. $CuMoO_4$ nanostructures exhibited significant deterioration under solar illumination due to the formation of active radicals, hence endorsing their use in visible-light technologies. Microwave-

assisted systems such as CuO@AC and CuO–CeO_2@AC provided rapid and efficient degradation in the absence of oxidants, indicating a viable and environmentally friendly method; nevertheless, infrastructural prerequisites may constrain scaling. $CuFe_2O_4$ demonstrated rapid disintegration under microwave radiation; nevertheless, the mechanisms of *N*-demethylation and intermediate stability required more scrutiny. Cu-doped ZnO nanoparticles exhibited enhanced degradation up to an ideal doping concentration, beyond which activity diminished, underscoring the necessity for meticulous doping regulation. Trimetallic Au/CuO/ZnO nanoparticles exhibited swift catalytic activity through plant-based production; yet, issues regarding reusability and nanoparticle durability persisted. The $CuCr_2O_4/SnO_2$ system facilitated effective sunlight-induced degradation by charge separation and transfer; however, its reliance on pH and precise dye concentrations constrained wider use. Although these materials demonstrated significant degrading efficiency, more efforts were required to address scalability, stability, cost-effectiveness, and evaluation in actual wastewater systems for practical use.

6. Adsorption method

Adsorption was a phenomenon gas or liquid molecules, atoms, or ions adhere to the surface of a solid body.[138] Surface association occurs when molecules develop weak van der Waals or chemical interactions with active areas. The adsorption process is the adhesion of a gaseous, liquid, or solid material known as the substrate to the surface of a solid or liquid known as the sorbent or adsorbent. There are two types of adsorption systems: liquid–liquid and liquid–gas.[139] The interfacial layer known as a film, micelle, or emulsion forms when a liquid substance acts as an adsorbent. Since the adsorbent is a solid substance, the interfacial layer model is the authorized mechanism for the adsorption process in the other system, which is solid–liquid or solid–gas. The equilibrium between the bulk phase and the adsorbent is described by the interfacial layer.[140] The substrate binds to the sorbent surface in the first region, while the sorbent's surface layer is in the second.

Table 2 outlined the synthesis conditions—temperatures marginally above room temperature ($\approx$60 °C), reaction times of about 3 h, and particle sizes between 10 and 70 nm—enabling researchers to understand the consistent fabrication of these nanoparticles and the influence of these parameters on final characteristics such as surface area and catalytic activity. Smaller nanoparticles often offer a greater surface area, hence enhancing dye removal efficiency. The predominance of adsorption studies aligning with the Langmuir isotherm and pseudo-second-order kinetics suggests that adsorption onto CuO and doped-CuO follows a consistent monolayer development on uniform surfaces, dictated by chemisorption. These models offer precise assessments of adsorption capacity and kinetics, crucial for the design of wastewater treatment systems and the transfer of laboratory findings to real-world scenarios. Comprehending the necessity for alkaline conditions provides a vital mechanistic insight: although CV is cationic, increasing the pH amplifies the negative surface charge on the adsorbent, hence strengthening electrostatic attraction and improving removal efficacy. This clarity enhances the optimization of treatment protocols and ensures consistency across several laboratories. Ultimately, distinguishing between dark adsorption and UV-vis-assisted photocatalysis reveals that researchers concentrate on both passive removal and active degradation. The requirement for light profoundly influences practical application: it determines energy needs, reactor design, and overall feasibility. This categorization, which includes nanoparticle production, size effects, adsorption models, pH conditions, and light dependency, provides a systematic framework. It allows researchers to quickly identify critical elements, uncover current shortcomings (*e.g.*, long-term stability, regeneration), and develop more efficient, scalable, and robust dye-removal techniques.

6.1 Monometallic

Abbasi *et al.*[141] showed CuBTC (BTC = 1,3,5-benzenetricarboxylate) metal–organic frameworks (MOFs) were synthesized using solid-state conditions and ultrasound irradiation and CV absorption. The size, shape, and volume of the pores have a direct impact on CuBTC's capacity to carry out the intended function in a given application. A complicated 3D channel system is formed by the face-centered crystal lattice of *Fm*3*m* symmetry formed by the copper-benzene carboxylate units.[146] The various adsorption isotherm types, these pores display distinct adsorption behaviors. Stated differently, the ultrasound-assisted techniques provide a reduction in surface area as determined by the decreased capacity for nitrogen adsorption. Guest molecules can be encapsulated in either M-CuBTC or U-CuBTC MOFs. The bulk structure with the absorption and release characteristics of the two distinct CuBTC MOF samples with regard to the two dyes, CV.[147] The host's absorption of the guest is most likely controlled by hydrogen bonds and other supramolecular interactions with the secondary building unit (SBU). The technique was favored because the visitor's adsorption was spontaneous and the entropy rose as the guest was adsorbed. Aqueous molecules envelop CuBTC and guest species in solution, interacting with them. Many of these interactions need to be interrupted for binding to take place. The solvent molecules in the solution gain greater freedom when the host and guest solvent molecules are removed, which raises the entropy and causes solvent–solvent bonds[148,149] to form both TGA and UV/vis spectroscopy were used to assess the dye concentration. As contact time grows, CuBTC's sorption capacity rises as well.

Li *et al.*[143] reported one of the metal–organic frameworks (MOFs), copper coordination polymer with dithiooxamide (H_2-dtoaCu), for its possible use in the adsorption removal of CV from solution. Strong covalent interactions[150,151] bind metal ions to a range of rigid, rod-like organic ligands to form MOFs, which are crystalline nanoporous materials. CV removal onto H_2dtoaCu as a function of adsorbent concentration. As the adsorbent concentration rose, it was found that the percentage of dye removal increased, reaching equilibrium at 1.2 mg mL^{-1}. The increase in the surface area of the adsorbent, increase the

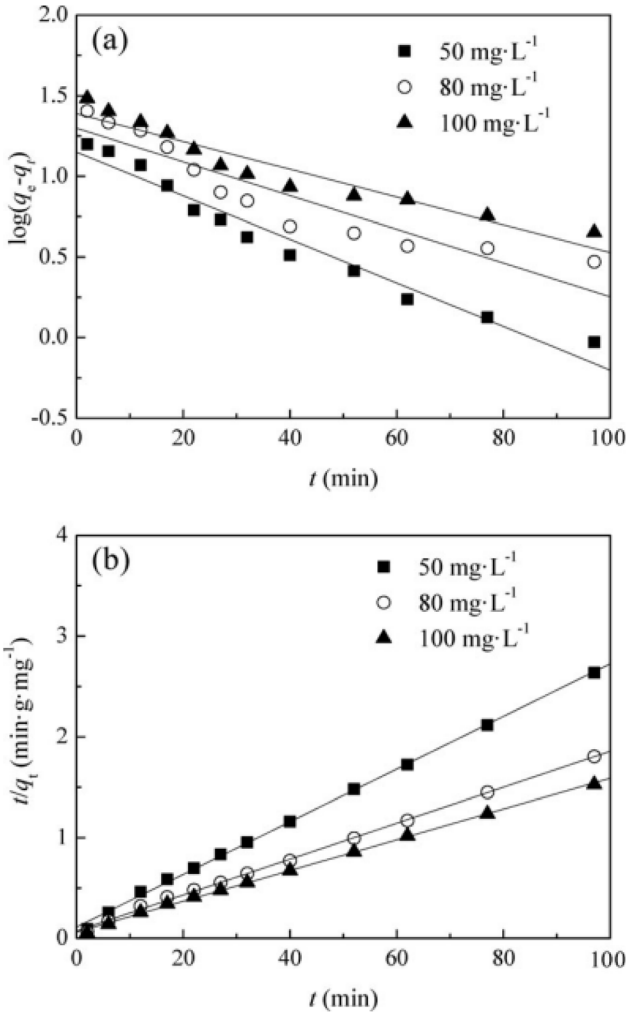

Fig. 11 Plots of (a) pseudo-first-order and (b) pseudo-second-order kinetic models for CV adsorption onto H_2 and Cu at various starting dye concentrations.[139]

number of adsorption sites that are accessible for adsorption.[152] The dye concentration and volume remain constant, the amount of dye adsorbed on H_2dtoaCu decreases as the adsorbent concentration rises. This could be brought on by adsorption sites overlapping or aggregating, which would reduce the overall adsorbent surface area available to dye and lengthen the diffusion path. Two kinetic models, pseudo-first-order and pseudo-second-order, used to study the adsorption process to determine the mechanism and possible rate-controlling processes involved in the adsorption of CV onto H_2dtoaCu. The pseudo first order eqn (16) pseudo second order eqn (17)

$$\log(q_e - q_t) = \log q_e - \frac{K_1}{2.303} t \quad (16)$$

$$\frac{t}{q_t} = \frac{1}{K_2 q_e^2} + \frac{t}{q_e} \quad (17)$$

q_e = the amount of dye adsorbed at equilibrium (mg g^{-1}) q_t = the amount of dye adsorbed at time t (mg g^{-1}) K_1 = pseudo first order rate constant (min^{-1}) K_2 = pseudo second order rate constant (g (mg $min)^{-1}$).

These equations showed that the correlation coefficients (R^2) for the pseudo-first-order kinetic model, acquired at various initial dye concentrations, fell between 0.8658 and 0.9616. This kinetic model yielded a wide range of theoretical and experimental equilibrium adsorption capabilities. The pseudo-first-order kinetic model is unable to explain the adsorption of CV on H_2dtoaCu.[153] The pseudo-second-order kinetic equation showed outstanding conformity with the kinetic data. Excellent linearity was demonstrated by the graphs of t/q_t against t of various initial dye concentrations. The correlation coefficients for the pseudo-second-order kinetic plots were all significantly higher than 0.9984 ($R^2 > 0.9984$), and the computed values of q_e coincided with experimental values quite well. The pseudo-second-order model's best correlation for the system indicates that chemisorption may be the rate-limiting phase for CV's sorption onto H_2dtoaCu. It was probable that valence forces would be involved in the adsorption behavior through the adsorbent and adsorbate sharing or exchanging electrons.[154] The pseudo-second-order rate constants for CV adsorption over H_2dtoaCu ($3.7 \times 10^{-3} \times -6.1 \times 10^{-3}$ g (mg $min^{-1})^{-1}$) are greater than those for the majority of the other adsorbents that have been reported, such as manganese oxide-coated sepiolite (0.15×10^{-3}–1.47×10^{-3} g (mg $min^{-1})^{-1}$), palm kernel fiber (0.35×10^{-3} g (mg $min^{-1})^{-1}$), and Cu(II)-loaded montmorillonite (3.5×10^{-3} g (mg $min^{-1})^{-1}$). The initial CV concentration rises, the kinetic constants over H_2dtoaCu marginally decrease. Comparable patterns of CV adsorption on palm kernel fiber and manganese oxide-coated sepiolite have been reported [Fig. 11].

Khani *et al.*[144] investigated Cu nanoparticles made from *Z. spina-christi* fruit extract can eliminate CV from aqueous solutions. After adding 0.1 M HCl or NaOH solution to bring the pH of this solution down to 9.0, 80 mg of the adsorbent (Cu-NPs). For 7.5 min, the solution is agitated to help the CV adhere to the Cu-NPs. Design-Expert version 7.0.0 software is used to perform an analysis of variance at a 95% confidence level to statistically evaluate the empirical model. The impact of the process factors on the percentage of CV removal from aqueous solutions by the Cu-NPs was investigated using eqn (1). The ANOVA data for the target dye indicates that the second-order polynomial model is very noteworthy and fits the experimental results well, as indicated by the models' P-value of < 0.0001 ($P < 0.05$) of CV. The three-dimensional response surface and contour graphs were created by solving the second polynomial equation. The regression equation used to get the best values for the variables. The combined effect of the dye's starting concentration and the pH of the solution on CV removal effectiveness at an adsorbent dosage of 80.0 mg. As the dye concentration decreased, the removal efficiency increased.[155] The Adsorbent's surface's increased number of binding sites. When the pH rises from 5.0 to 9.0, the elimination percentage increases. At all concentration levels, the maximum adsorption occurs at pH 9.0. As the solution's pH increases, more negatively charged sites appear. The adsorption of dye cations increases because of electrostatic attraction. Because the large dye ions became more mobile, extending the stirring time from 4 to 8 minutes enhanced CV's removal efficiency.[156,157] The amount of dye sorption rises with stirring time

due to increased affinity of dye sites or an increase in the number of binding sites on the absorbent. Because of its tiny particle size and high specific surface area, the adsorbent's percentage removal increases as dose increases. At higher levels, the rate of adsorption increased considerably due to increased surface area and the availability of more active adsorbing sites.[158]

Shukla *et al.*[145] employed a novel nanobiocomposite adsorbent, which is made by impregnating copper nanoparticles in the natural polymer chitosan, to remove color from aqueous media. The maximal monolayer adsorption capacity[159] (q_m) of copper nanoparticles impregnated in biocomposites (Cu/chit-NBC) was determined to be 84.75 mg g^{-1} by the Langmuir isotherm. The computed corresponding Langmuir adsorption constant (K_L) was 0.352 L mg^{-1}, falling between the permissible range of 0 and 1. The predicted constants for the heterogeneity factor ($1/n$) and Freundlich adsorption isotherm (K_F) were 0.616 and 5.291 mg g^{-1}, respectively. The sorption capacity is indicated by the K_F value, and the process's favorability or surface heterogeneity is predicted by the slope ($1/n$) of the Freundlich isotherm.[160,161] $1/n$ should have a value between 0 and 1. Greater surface heterogeneity is indicated by a value nearer zero. The computed "$1/n$" value showed that the produced nanobiocomposite had a moderate level of surface heterogeneity.[162] The Temkin isotherm model's linear fitting is shown. The Temkin parameters RT/b_T and AT, which stand for the enthalpy of adsorption and equilibrium binding constant, respectively, were calculated to be 17.958 kJ mol^{-1} and 1.914 L g^{-1}.[163] The Frisch isotherm model was found to be a good fit for the current study based on a comparison of the regression coefficient (R^2) for the three model.

6.2 Bimetallic

Abdel-Aziz *et al.*[142] produced bimetallic nano zero-valent iron-copper (Fe^0–Cu), algae-activated carbon, and their composites (AC–Fe^0–Cu) for use as adsorbents. Synthetic adsorbents are synthesized and evaluated for their capacity to adsorb and eliminate soluble cationic CV dye. The effect of synthetic adsorbents on the adsorption and elimination of soluble cationic CV dye, utilizing UV-vis spectroscopy across varying pH levels (3–10), time intervals (15–180 minutes), and starting dye concentrations (50–500 ppm). Untreated algae demonstrate a remarkable 96.64% removal effectiveness under the specified conditions: pH 7, a contact duration of 180 minutes, a rotating speed of 120 rpm, a temperature range of 25 °C to 30 °C, a concentration of 300 ppm in the CV dye solution, and an adsorbent dosage of 4 g L^{-1} of raw algae. The optimal removal efficiencies of raw algae Fe^0–Cu and H_3PO_4 chemical AC–Fe^0–Cu are 97.61% and 97.46%, respectively, at a pH of 7, a contact time of 150 minutes, a rotational speed of 120 rpm, a temperature range of 25–30 °C, a concentration of 75 ppm of CV dye solution, and doses of 1.5 g L^{-1} for raw algae Fe^0–Cu adsorbent and 1 g L^{-1} for H_3PO_4 chemical AC–Fe^0–Cu adsorbent.

6.2.1 Critical analysis. The investigations collectively illustrate the efficacy of copper-based materials for the removal of CV dye, while also highlighting significant limits. Li *et al.*[143] H_2dtoaCu exhibits robust chemisorption characterized by pseudo-second-order kinetics; nevertheless, efficiency diminishes at elevated adsorbent concentrations due to aggregation and a decrease in active surface area. Khani *et al.*[144] Cu-NPs demonstrate rapid removal and great efficacy at pH 9; nevertheless, their brief contact duration and restricted pH range pose questions regarding practical application. Shukla *et al.*[145] Cu/chitosan nanobiocomposite demonstrates substantial adsorption capacity and reusability, exhibiting a favorable isotherm fit; nevertheless, considerable surface heterogeneity and the absence of interference studies may restrict its practical use. Abbasi *et al.*[141] CuBTC metal–organic frameworks, although providing intricate porous architectures and entropy-driven adsorption, encounter difficulties related to surface area reduction during ultrasonic synthesis and possible instability under fluctuating circumstances. In summary, although these materials show potential, more efforts are required to overcome their operating constraints, compatibility with actual wastewater, and long-term durability.

7. Mechanism of adsorption

7.1 Electrostatic attraction

Electrostatic interactions are fundamental forces that arise from the attraction or repulsion between particles carrying electric charges. These interactions are governed by Coulomb's law, which states that the force between two point charges is directly proportional to the product of their charges and inversely proportional to the square of the distance between them.[164] Such forces are central to numerous phenomena in physics, chemistry, and biology. In the realm of materials science and nanotechnology, electrostatic interactions are harnessed to manipulate and assemble nanoscale structures. For example, electrostatic forces are utilized in the design of electroadhesive devices, where an electric field induces adhesion between surfaces. This principle is applied in various technologies, including robotic grippers and electronic displays.[165,166]

Functional groups containing oxygen are present in Fe^0–Cu, which will raise the surface charge density and enable the creation of hydrogen bonds with reactive oxygen. CV and the adsorbent surface interact electrostatically. The negatively charged surface of Fe^0–Cu nanocomposites encourages electrostatic attraction to the cationic CV through an ion exchange adsorption mechanism.[119]

7.2 π–π stacking interactions

π–π stacking, also known as pi stacking, refers to noncovalent interactions between aromatic rings, primarily driven by the overlap of their π-electron clouds. Contrary to the term "stacking," which might suggest a direct superimposition of rings (sandwich configuration), such arrangements are often electrostatically repulsive due to the alignment of like-charged regions. Instead, more stable configurations involve offset arrangements, such as parallel-displaced or T-shaped geometries, where electrostatic attractions between partial charges on hydrogen and carbon atoms enhance stability.[167,168]

Additionally, adsorption is facilitated by the π–π stacking interactions between the nanoparticle's surface and the

aromatic rings of CV, especially with Fe^0–Cu nanoparticles that have a large surface area because of which about 20% of the dye was eliminated.[169]

Shukla *et al.*[145] state that the probable mechanism of CV dye adsorption by the produced nano bio composite was assessed using the chemical composition of the nano bio composite, kinetics, and adsorption isotherm discovered during the experiment. The Cu/chit-NBC surface was dominated by negatively charged functional groups such as carboxylate and hydroxyl, as confirmed by FT-IR peaks. At pH > 7, they remained in an ionized form as well. Adsorbed H^+ ions would be negligible. The presence of comparatively stronger connections between dyes and nanobio composite (NBC) molecules, such as electrostatic contact, H-bonding, or π–π interaction, was indicated by pseudo-second order kinetics of dye adsorption. The cationic dye CV was trapped on the surface of the Cu/chit-NBC nano bio composite by interactions enhanced by –OH (hydroxyl), –COOH (carboxylic), $–NH_2$ (amine), or –NH–CH– (imine) groups surface or within its pores.

7.3 Internal and external adsorbing

The Langmuir model is the best fit for the chemisorptive nature of CV adsorption on Fe^0–Cu. A pseudo-second-order kinetic model, which further validates chemisorption. An $\left(\frac{1}{n}\right)$ value of 0.8449 indicates that adsorption is favored, driven by spontaneous adsorption and an increase in entropy. CV can be strongly adsorbed by Fe-based adsorbents.[170,171] The remarkable performance of nano zero valent iron (nZVI) and bimetallic Fe^0–Cu adsorbents is linked to their effective reduction capacities. Adsorbents based on iron decrease and remove CV from solutions. When compared to adsorbents made with monovalent metals, those made with bivalent metals demonstrated a higher adsorption affinity for pollutants. Consequently, the presence of copper and iron ions in combination with bimetallic adsorbents improves adsorption effectiveness, whereas the addition of activated carbon promotes the recyclable and reusable nature of the nanocomposites.[142] The adsorption capacity, kinetics, surface reactions, porosity, and regeneration potential of adsorbent materials are all significantly influenced by the specific surface area. When choosing or creating adsorbent materials for a variety of applications, a greater specific surface area is crucial because it is usually linked to improved adsorption.[128] The adsorbent and adsorbate interact during the adsorption process. More active sites and surface reactions are made possible by a larger surface area, which enhances adsorption effectiveness. Furthermore, a higher specific surface area improves desorption processes by facilitating the more efficient removal of adsorbate molecules during heat regeneration, which increases the adsorbent's lifetime and recyclability.[172]

8. Antibacterials properties

The effectiveness of several widely used antibiotics against certain infections has decreased over the past few decades, though, not only because many of them cause harmful effects but also because drug-resistant bacteria have emerged. Researching more recent medications with lower resistance is crucial.[173] Natural source-based medications are important for both treating and preventing human illnesses. Traditional medicine is one of the main healthcare systems in many poor nations. The use of herbs in traditional medicine is widespread. Showed the release of copper ions, which stick to and damage the bacterial cell wall and cause the lysis of the bacterial cell, is most likely the mechanism by which Cu NCs have an antibacterial effect. Gram-positive and Gram-negative bacteria differ in their cell wall thickness, which accounts for their differences in activity.[174] Using a membrane damage assay, the effects of copper–nickel hybrid nanoparticles on the bacterial cell membranes' integrity were investigated. Every time nanoparticles come into touch with the bacterial cell membrane, internal components are released outside. The bacterial strains were ultimately eliminated because damaged membranes were unable to transport the contents of the cells.[95] In comparison to the conventional antibiotic, the textiles treated with CuONPs exhibited reduced antibacterial activity against *E. coli* and increased antibacterial activity against *S. aureus* and *K. pneumoniae*. Khani *et al.*[144] reported using the agar well-diffusion method on nutrient agar (NA) plates, the bactericidal activity of methanolic and aquatic fruit extract, $CuSO_4$ solution, and biosynthesized Cu-NPs at four different concentrations (25, 50%, 75%, and 100% v/v) is assessed. The antibacterial assay uses *Escherichia coli* (Gram-negative) and *Staphylococcus aureus* (Gram-positive) as references. These two treatments are used in two replicates of the experiment. Using the sterile tip, the wells (diameter = 7 mm) are punched over the agar plates. The sterile cotton swab is used to swab the cultures on the test plates. After inoculating the holes with 80 μL of each sample at different doses, they are incubated for 48 hours at 37 °C. Following the incubation period, the growth inhibition zones' diameter is measured using a scale and reported in centimeters.

9. pH effect

It is observed that at all concentration levels, the greatest adsorption occurs at pH 9.0. As the pH of the solution rises, there are more negatively charged sites.[144] Because of the electrostatic attraction, this causes the adsorption of dye cations increases.[145] The CV decoloration increased from 40.3% to 91.5% when the pH was raised from 4 to 7. The adsorption effectiveness to 67.5% when the pH was raised to 10. This action could potentially be the result of electrostatic magnetism or disgust between the NBC and CV dye molecules. The adsorption and desorption of CV molecules are significantly impacted by the surface charges of the NBC adsorbent. The pH 7–8 range is ideal for CV deterioration, according to most of the research.

10. Reusability

Peddada *et al.*[12] used CuO nanoparticle for removal of CV. After every degradation process, the catalyst was cleaned with alcohol and double-distilled water to remove any color that had adhered

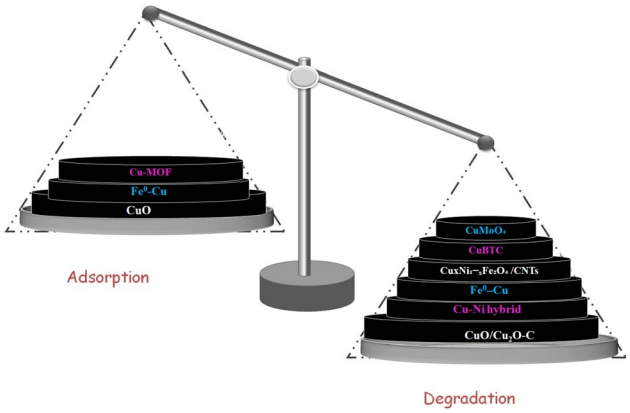

Fig. 12 Comparison between adsorption and degradation for CV removal.

to the surface and it was then oven-dried for future usage. After five cycle the catalyst remain stable and applicable for the dye degradation.[169] Reported Fe^0–Cu bimetallic for CV removal by serving as an oxidation process catalyst, the Cu component increases the nanocomposites' reusability. The surface characteristics of the adsorbent can be altered by adding functional groups and chemicals such as H_2SO_4 and H_3PO_4, which increase the active sites and adsorption selectivity for the target dye and activated carbon was a key reason for enhanced reusability. Shukla *et al.*[145] used the cu chitosan nano-biocomposite catalyst for degradation even after regeneration, its decolorization efficiency remained encouraging. In aqueous CV media, even after the seventh regeneration cycle, Cu/chit-NBC maintained a decolorization effectiveness of over 80%. Up until the eleventh cycle of decolorization, about 50% of the efficiency was maintained. The above result mentioned that Shukla *et al.* showed the best efficiency for the CV dye removal.

11. Circular economy

Circular economy is the use of waste materials from different industry household and other materials into the environmental remediation.[175] It was highly recommended to use wastes as precursors, as this promotes the circular economy by elevating many wastes for the sustainable management of pollutants, atrazine removal must integrate the circular economy. Commercially available activated carbon effectively removes contaminants from water through atrazine adsorption because of its microporosity, a large specific surface area, and insensitivity to dangerous contaminants.[176] Utilizing copper oxide nanoparticles to break down malachite green dye offers a potential chance to adhere to the circular economy's tenets. The suggested method has a number of advantages over traditional color removal techniques, according to a cost-benefit study. Using a green method to synthesize CuO-NPs from e-waste significantly lowers the cost of acquiring raw materials. Researchers reduce waste and production expenses by reusing copper sulfate that is taken from discarded electronic materials. Furthermore, using banana blossom extract as a reducing agent lessens the requirement for pricey chemical reagents while also aiding in the biosynthetic process.[177] A circular economy strategy by using industrial metal scrap as a raw material to make nanoparticles and a simple electrochemical method to produce iron oxide nanoparticles. Iron oxide nanoparticle particularly absorbed the Congo red dye from an aqueous solution. Abdel-Aziz *et al.*[169] and Abdullah *et al.*[85] used agro-biomass wheatgrass extract, fava bean, *Zingiber officinale* rhizome extract for CV dye removal those were green synthesized and does not produce harmful product and also does environmental remediation. Those were facile green synthesized, bio compatible, cheap, ecofriendly, reusable in nature.

12. Degradation *vs.* adsorption

The removal of CV, a cationic dye prevalent in industrial effluents, is crucial due to its toxicity and environmental persistence.[178] Copper-based nanoparticles (Cu-NPs) have been extensively studied for CV removal through two primary mechanisms: adsorption and degradation. This comprehensive analysis compares these methods, highlighting their mechanisms, efficiencies, and practical considerations. Adsorption involves the accumulation of dye molecules onto the surface of an adsorbent.[179] Copper-based nanoparticles, such as copper ferrite ($CuFe_2O_4$), exhibit high surface areas and magnetic properties, facilitating efficient dye adsorption and easy separation from aqueous solutions. The adsorption process is influenced by factors like pH, contact time, and nanoparticle surface characteristics.[180] For instance, copper ferrite nanoparticles synthesized *via* a green combustion method using succinic and malic acids demonstrated high adsorption capacities for CV. At pH 10, the removal efficiency reached up to 85.83%, with adsorption capacities of 429.16 mg g^{-1}. The process followed pseudo-second-order kinetics and fitted well with the Langmuir isotherm model, indicating monolayer adsorption on a homogeneous surface. Degradation, on the other hand, involves breaking down dye molecules into less harmful substances.[13] Copper-based nanoparticles act as catalysts in processes like photocatalysis and catalytic wet peroxide oxidation (CWPO), generating reactive oxygen species (ROS) that oxidize dye molecules. For example, under visible light irradiation, CuS nanoparticles achieved up to 84.6% degradation efficiency for CV.[181] In CWPO processes, mixed manganese–copper oxides facilitated complete degradation of CV within 150 minutes, significantly reducing chemical oxygen demand (COD) and total organic carbon (TOC). Additionally, green-synthesized CuO nanoparticles using *Ruellia tuberosa* extract demonstrated effective photocatalytic degradation of CV under sunlight [Fig. 12].

Both adsorption and degradation using copper-based nanoparticles are effective methods for the removal of CV from aqueous solutions. The choice between the two depends on specific treatment goals, operational capabilities, and environmental considerations.[182] Adsorption is suitable for scenarios where quick removal is needed and facilities are available for handling and regenerating spent adsorbents.[128] Degradation is preferable when complete elimination of dye molecules is desired and there is access to necessary conditions (*e.g.*, light sources, oxidants) for catalytic processes. In practice, a combination of

both methods may offer a comprehensive solution, leveraging the rapid removal capabilities of adsorption and the thorough pollutant breakdown achieved through degradation.

13. Conclusions and future scope

Dye production and use have increased recently, leading to a rise in environmental pollution. Different methods have been used to get rid of dyes. Nevertheless, a workable and affordable solution for eliminating all dyes has not yet been developed. The findings of the aforementioned literature and the techniques used in the study's lead to the conclusion that, for the removal of CV using biomaterials, a collection or combination of various adsorption-based processes produces fruitful results. However, it is also noted that there are certain disadvantages to biosorption, as despite their upright efficiency and applicability, an economic consideration has limited the use of certain varieties because regeneration processes result in a significant loss of adsorbent. Industrial wastewater treatment has been increasingly important in recent years, as rules have become harsher and researchers have long demonstrated the negative effects improper treatment may have on human health, safety, and the environment before final release. Lastly, based on the information found in the literature, CV removal can be partially accomplished using inexpensive adsorbents because they have several benefits, many of which are renewable and readily available natural resources currently in use. Atomically precise metal nanoclusters (NCs) are ultrasmall particles with less than 2 nm core diameters that fall between the atomic and plasmonic metal nanoparticles.[183,184] Such fluorescent nanoclusters are currently an active field of research concerning dye degradation because of the extraordinarily high surface-to-volume ratio. The employment of nanoclusters for the elimination of CV is not available in the literature. More research is warranted for nanocluster-induced CV dye removal.[25] This review article illustrates dye degradation, adsorption, mechanism, and antibacterial properties. It is hoped that it will help young researchers who are pursuing environmental nanoscience to address current environmental issues.

Author contributions

Supriyo Kar and Priyanka Sharma reviewed the literature and wrote a major part of the manuscript. Mainak Ganguly, the corresponding author, designed and edited the manuscript. Mamta Sahu reviewed and wrote some parts of the manuscript. Supriyo Kar and Priyanka Sharma both will be considered as first author for the present manuscript.

Conflicts of interest

There is no competing interest to disclose.

Data availability

No primary research results, software or code have been included and no new data were generated or analysed as part of this review.

References

1 J. O. Ighalo, P. A. Sagboye, G. Umenweke, O. J. Ajala, F. O. Omoarukhe, C. A. Adeyanju, S. Ogunniyi and A. G. Adeniyi, *Environ. Nanotechnol. Monit. Manag.*, 2021, **15**, 100443.
2 M. Narayanan, S. H. Salmen, A. Chinnathambi, K. Suresh, Ramesh, S. Barathi and J. Lee, *J. Taiwan Inst. Chem. Eng.*, 2025, **166**, 105258.
3 S. Lata and Siddharth, *Energy Nexus*, 2021, **3**, 100020.
4 T. A. Aragaw, *J. Hazard. Mater. Adv.*, 2024, **16**, 100493.
5 B. Lellis, C. Z. Fávaro-Polonio, J. A. Pamphile and J. C. Polonio, *Biotechnol. Res. Innov.*, 2019, **3**, 275–290.
6 S. Dutta, S. Adhikary, S. Bhattacharya, D. Roy, S. Chatterjee, A. Chakraborty, D. Banerjee, A. Ganguly, S. Nanda and P. Rajak, *J. Environ. Manage.*, 2024, **353**, 120103.
7 P. Sathish Kumar, B. Shobana and P. Prakash, *Chemosphere*, 2024, **354**, 141708.
8 J. Balasubramanian, S. K. Ponnaiah, P. Periakaruppan and D. Kamaraj, *Environ. Sci. Pollut. Res. Int.*, 2020, **27**, 2328–2339.
9 A. Ayub, A. K. Wani, C. Chopra, D. K. Sharma, O. Amin, A. W. Wani, A. Singh, S. Manzoor and R. Singh, *Bacteria*, 2025, **4**, 15.
10 N. Ramesh, C. W. Lai, M. R. B. Johan, S. M. Mousavi, I. A. Badruddin, A. Kumar, G. Sharma and F. Gapsari, *Heliyon*, 2024, **10**, e40998.
11 S. K. Ponnaiah, P. Periakaruppan, B. Vellaichamy and B. Nagulan, *J. Colloid Interface Sci.*, 2018, **512**, 219–230.
12 L. M. Peddada, P. Phyu Cho, S. Dulgaj, R. Annapragada and P. Raja Kanuparthy, *Results. Opt.*, 2023, **13**, 100537.
13 S. Khan, T. Noor, N. Iqbal and L. Yaqoob, *ACS Omega*, 2024, **9**, 21751–21767.
14 P. Sathish Kumar, P. Periakaruppan, T. Arumuganathan and B. Jeyaprabha, *J. Photochem. Photobiol., A*, 2019, **380**, 111860.
15 A. Chakravorty and S. Roy, *Sustain. Chem. Environ.*, 2024, **8**, 100155.
16 J. Zhang, H. Wu, L. Shi, Z. Wu, S. Zhang, S. Wang and H. Sun, *Sep. Purif. Technol.*, 2024, **329**, 125225.
17 H. Kumari, S. Sonia, R. Ranga, S. Chahal, S. Devi, S. Sharma, S. Kumar, P. Kumar, S. Kumar, A. Kumar and R. Parmar, *Water Air Soil Pollut.*, 2023, **234**, 349.
18 R. Agarwala and L. Mulky, *ChemBioEng Rev.*, 2023, **10**, 326–335.
19 M. Gayathiri, T. Pulingam, K. T. Lee and K. Sudesh, *Chemosphere*, 2022, **294**, 133764.
20 M. Liu, J. Zheng, L. Wang, Z. Hu, S. Lan, W. Rao, Y. Liu, Y. Xie and C. Yu, *J. Mol. Struct.*, 2022, **1263**, 133150.
21 R. Suresh, L. Gnanasekaran, S. Rajendran, A. A. Jalil, M. Soto-Moscoso, K. S. Khoo, Z. Ma, H. S. Halimatul Munawaroh and P. L. Show, *Chemosphere*, 2023, **343**, 140173.
22 M. T. Yagub, T. K. Sen, S. Afroze and H. M. Ang, *Adv. Colloid Interface Sci.*, 2014, **209**, 172–184.

23 E. Murugan, J. Nimita Jebaranjitham, K. Janaki Raman, A. Mandal, D. Geethalakshmi, M. Dharmendira Kumar and A. Saravanakumar, *New J. Chem.*, 2017, **41**, 10860–10871.
24 N. P. Raval, P. U. Shah and N. K. Shah, *Appl. Water Sci.*, 2017, **7**, 3407–3445.
25 P. Sharma, M. Ganguly and M. Sahu, *RSC Adv.*, 2024, **14**, 11411–11428.
26 C. Osagie, A. Othmani, S. Ghosh, A. Malloum, Z. Kashitarash Esfahani and S. Ahmadi, *J. Mater. Res. Technol.*, 2021, **14**, 2195–2218.
27 S. Raina, A. Roy and N. Bharadvaja, *Environ. Nanotechnol. Monit. Manag.*, 2020, **13**, 100278.
28 R. Sarathi, N. L. Sheeba, E. Selva Essaki and S. Meenakshi Sundar, *Mater. Today: Proc.*, 2022, **64**, 1859–1863.
29 A. I. Khedr and M. H. H. Ali, *Sci. Rep.*, 2024, **14**, 29156.
30 S. C. Priya, S. Vijayalakshmi, S. G. Raghavendra, S. Yıldızhan and J. Ranjitha, *Mater. Today: Proc.*, 2023, **80**, 3075–3081.
31 M. Sifat, E. Shin, A. Schevon, H. Ramos, A. Pophali, H.-J. Jung, G. Halada, Y. Meng, N. Olynik, D. J. Sprouster and T. Kim, *Catalysts*, 2024, **14**, 377.
32 S. Mani and R. N. Bharagava, in *Reviews of Environmental Contamination and Toxicology*, ed. W. P. de Voogt, Springer International Publishing, Cham, 2016, vol. 237, pp. 71–104, DOI: 10.1007/978-3-319-23573-8_4.
33 Z. Moradi, S. Z. Jahromi and M. Ghaedi, in *Interface Science and Technology*, ed. M. Ghaedi, Elsevier, 2021, vol. 32, pp. 557–623.
34 A. O. Ibhadon and P. Fitzpatrick, *Catalysts*, 2013, **3**, 189–218.
35 W. Au, S. Pathak, C. J. Collie and T. C. Hsu, *Mutat. Res. Genet. Toxicol.*, 1978, **58**, 269–276.
36 Y. Luo, W. Guo, H. H. Ngo, L. D. Nghiem, F. I. Hai, J. Zhang, S. Liang and X. C. Wang, *Sci. Total Environ.*, 2014, **473–474**, 619–641.
37 J. T. Alexander, F. I. Hai and T. M. Al-aboud, *J. Environ. Manage.*, 2012, **111**, 195–207.
38 I. Sirés and E. Brillas, *Environ. Int.*, 2012, **40**, 212–229.
39 Z.-b. Zhang, Z.-w. Zhou, X.-h. Cao, Y.-h. Liu, G.-x. Xiong and P. Liang, *J. Radioanal. Nucl. Chem.*, 2014, **299**, 1479–1487.
40 S. Sharma, A. O. Ibhadon, M. G. Francesconi, S. K. Mehta, S. Elumalai, S. K. Kansal, A. Umar and S. Baskoutas, *Nanomaterials*, 2020, **10**, 910.
41 P. Gao, Y. Yang, Z. Yin, F. Kang, W. Fan, J. Sheng, L. Feng, Y. Liu, Z. Du and L. Zhang, *J. Hazard. Mater.*, 2021, **412**, 125186.
42 J. Rivera-Utrilla, M. Sánchez-Polo, M. Á. Ferro-García, G. Prados-Joya and R. Ocampo-Pérez, *Chemosphere*, 2013, **93**, 1268–1287.
43 D. T. Ruziwa, A. E. Oluwalana, M. Mupa, L. Meili, R. Selvasembian, M. M. Nindi, M. Sillanpaa, W. Gwenzi and N. Chaukura, *J. Water Proc. Eng.*, 2023, **54**, 103880.
44 A. L. Onugwu, C. S. Nwagwu, O. S. Onugwu, A. C. Echezona, C. P. Agbo, S. A. Ihim, P. Emeh, P. O. Nnamani, A. A. Attama and V. V. Khutoryanskiy, *J. Controlled Release*, 2023, **354**, 465–488.
45 J. Pavlović, Z. Farkas, L. Kraková and D. Pangallo, *Appl. Sci.*, 2022, **12**, 9991.
46 F. Rehman, M. Sayed, J. Khan and H. Khan, *J. Chil. Chem. Soc.*, 2017, **1**, 3359–3364.
47 H.-J. Fan, S.-T. Huang, W.-H. Chung, J.-L. Jan, W.-Y. Lin and C.-C. Chen, *J. Hazard Mater.*, 2009, **171**, 1032–1044.
48 J. L. Allen and J. R. Meinertz, *J. Chromatogr. A*, 1991, **536**, 217–222.
49 M. R. Hassan, S. M. Yakout, A. A. Abdeltawab and M. I. Aly, *J. Saudi Chem. Soc.*, 2021, **25**, 101231.
50 S. Mechati, M. Zamouche, H. Tahraoui, O. Filali, S. Mazouz, I. N. E. Bouledjemer, S. Toumi, Z. Triki, A. Amrane, M. Kebir, S. Lefnaoui and J. Zhang, *Water*, 2023, **15**, 4274.
51 O. A. Logutenko, A. I. Titkov, A. M. Vorobyov and N. Z. Lyakhov, *J. Mater. Res. Technol.*, 2021, **13**, 1254–1265.
52 S. Meghana, P. Kabra, S. Chakraborty and N. Padmavathy, *RSC Adv.*, 2015, **5**, 12293–12299.
53 R. K. Ameta, P. Malik, S. Korgaokar, P. Vanzara and K. Soni, *Plant Nano Biol.*, 2024, **7**, 100065.
54 K. Hua, Y. Shi, M. Tang, X. Zuo, J. Gao and X. Zhang, *Colloids Surf., A*, 2024, **698**, 134605.
55 P. U. Nzereogu, A. D. Omah, F. I. Ezema, E. I. Iwuoha and A. C. Nwanya, *Appl. Surf. Sci. Adv.*, 2022, **9**, 100233.
56 M. F. Al-Hakkani, *SN Appl. Sci.*, 2020, **2**, 505.
57 A. Antonio-Pérez, L. F. Durán-Armenta, M. G. Pérez-Loredo and A. L. Torres-Huerta, *Micromachines*, 2023, **14**, 1882.
58 M. C. Crisan, M. Teodora and M. Lucian, *Appl. Sci.*, 2022, **12**, 141.
59 M. B. Gawande, A. Goswami, F.-X. Felpin, T. Asefa, X. Huang, R. Silva, X. Zou, R. Zboril and R. S. Varma, *Chem. Rev.*, 2016, **116**, 3722–3811.
60 M. Pourmadadi, R. Holghoomi, A. shamsabadipour, R. Maleki-baladi, A. Rahdar and S. Pandey, *Plant Nano Biol.*, 2024, **8**, 100070.
61 J. Jiang, P. Zhang, Y. Liu and H. Luo, *Anal. Methods*, 2017, **9**, 2205–2210.
62 N. Tuccitto, L. Riela, A. Zammataro, L. Spitaleri, G. Li-Destri, G. Sfuncia, G. Nicotra, A. Pappalardo, G. Capizzi and G. Trusso Sfrazzetto, *ACS Appl. Nano Mater.*, 2020, **3**, 8182–8191.
63 S. Gao, Q. Wang, H. Guo, X. Liu, G. Li, L. Dong and K. Song, *J. Mater. Res. Technol.*, 2023, **24**, 2346–2356.
64 L. Yuan, M. Liang, M. Hummel, C. Shao and S. Lu, *Chemosensors*, 2023, **11**, 159.
65 V. Subha, S. Kirubanandan, M. Arulmozhi and S. Renganathan, *Chemist*, 2018, **91**, 9–19.
66 J. Möbs, J.-N. Luy, A. Shlyaykher, R. Tonner and J. Heine, *Dalton Trans.*, 2021, **50**, 15855–15869.
67 V. Seerangaraj, S. Sathiyavimal, S. N. Shankar, J. G. T. Nandagopal, P. Balashanmugam, F. A. Al-Misned, M. Shanmugavel, P. Senthilkumar and A. Pugazhendhi, *J. Environ. Chem. Eng.*, 2021, **9**, 105088.
68 A. H. AbdEl-Salam, H. A. Ewais and A. S. Basaleh, *J. Mol. Liq.*, 2017, **248**, 833–841.
69 S. H. Al-Ansari, H. Gomaa, R. D. Abdel-Rahim, G. A. M. Ali and A. M. Nagiub, *Sci. Rep.*, 2024, **14**, 4379.

70 R. Goswami, M. Gogoi, H. J. Borah, P. G. Ingole and S. Hazarika, *J. Environ. Chem. Eng.*, 2018, **6**, 6139–6146.
71 P. Raizada, A. Sudhaik, S. Patial, V. Hasija, A. A. Parwaz Khan, P. Singh, S. Gautam, M. Kaur and V.-H. Nguyen, *Arab. J. Chem.*, 2020, **13**, 8424–8457.
72 K. Naseem, Z. H. Farooqi, R. Begum, W. Wu, A. Irfan and A. G. Al-Sehemi, *Macromol. Chem. Phys.*, 2018, **219**, 1800211.
73 K. H. Hama Aziz, H. Miessner, S. Mueller, A. Mahyar, D. Kalass, D. Moeller, I. Khorshid and M. A. M. Rashid, *J. Hazard. Mater.*, 2018, **343**, 107–115.
74 M. Anari-Anaraki and A. Nezamzadeh-Ejhieh, *J. Colloid Interface Sci.*, 2015, **440**, 272–281.
75 A. Nezamzadeh-Ejhieh and M. Kabiri-Samani, *J. Hazard. Mater.*, 2013, **260**, 339–349.
76 A. Nezamzadeh-Ejhieh and M. Karimi-Shamsabadi, *Chem. Eng. J.*, 2013, **228**, 631–641.
77 A. R. Hernandez-Martínez, J. A. Lujan-Montelongo, C. Silva-Cuevas, J. D. Mota-Morales, M. Cortez-Valadez, Á. d. J. Ruíz-Baltazar, M. Cruz and J. Herrera-Ordonez, *React. Funct. Polym.*, 2018, **122**, 75–84.
78 F. Salimi, S. S. Emami and C. Karami, *Inorg. Nano-Met. Chem.*, 2018, **48**, 31–40.
79 F. Salimi, M. Eskandari and C. Karami, *Desalination Water Treat.*, 2017, **85**, 206–214.
80 H. Derikvandi and A. Nezamzadeh-Ejhieh, *J. Colloid Interface Sci.*, 2017, **490**, 628–641.
81 M. Nasrollahzadeh, Z. Issaabadi and S. M. Sajadi, *RSC Adv.*, 2018, **8**, 3723–3735.
82 H. Kolya and C. W. Kang, *Toxics*, 2024, **12**, 111.
83 G. R. Aiken, H. Hsu-Kim and J. N. Ryan, *Environ. Sci. Technol.*, 2011, **45**(8), 3196–3201.
84 D. A. Bopape, B. Ntsendwana and F. D. Mabasa, *Heliyon*, 2024, **10**, e39316.
85 Abdullah, T. Hussain, S. Faisal, M. Rizwan, Saira, N. Zaman, M. Iqbal, A. Iqbal and Z. Ali, *J. Saudi Chem. Soc.*, 2022, **26**, 101486.
86 M. Dhara, A. Karmakar, K. Kisku and S. K. Ganesan, *Research Square*, 2022, DOI: 10.21203/rs.3.rs-1970462/v1.
87 R. Dobrucka, *Int. J. Environ. Anal. Chem.*, 2021, **101**, 2046–2057.
88 A. Jamil, *J. Taibah Univ. Sci.*, 2021, **15**, 814–825.
89 H. Chen, S. Yang, J. Chang, K. Yu, D. Li, C. Sun and A. Li, *Chemosphere*, 2012, **89**, 185–189.
90 J. Yin, J. Cai, C. Yin, L. Gao and J. Zhou, *J. Environ. Chem. Eng.*, 2016, **4**, 958–964.
91 Somnath, M. Ahmad and K. A. Siddiqui, *ACS Omega*, 2022, **7**, 41120–41136.
92 A. Mahmood, S. Din, A. Khan, A. Bukhari, K. Zeb and S. Khan, *Room Temperature Assisted Copper Selenide Based Composite for Outstanding Crystal Violet Degradation*, 2024.
93 H. Lahmar, M. Benamira, S. Douafer, F. Z. Akika, M. Hamdi, I. Avramova and M. Trari, *Optik*, 2020, **219**, 165042.
94 M. Mittal, M. Sharma and O. P. Pandey, *Sol. Energy*, 2014, **110**, 386–397.
95 S. Vasantharaj, S. Sathiyavimal, M. Saravanan, P. Senthilkumar, K. Gnanasekaran, M. Shanmugavel, E. Manikandan and A. Pugazhendhi, *J. Photochem. Photobiol., B*, 2019, **191**, 143–149.
96 S. Sukumar, A. Rudrasenan and D. Padmanabhan Nambiar, *ACS Omega*, 2020, **5**, 1040–1051.
97 A. F. Zedan, A. T. Mohamed, M. S. El-Shall, S. Y. AlQaradawi and A. S. AlJaber, *RSC Adv.*, 2018, **8**, 19499–19511.
98 D. Gupta, S. R. Meher, N. Illyaskutty and Z. C. Alex, *J. Alloys Compd.*, 2018, **743**, 737–745.
99 N. M. R. Mahmoud, H. I. Mohamed, S. B. Ahmed and S. Akhtar, *Chem. Pap.*, 2020, **74**, 2825–2835.
100 E. A. A. El-Shazly, S. I. Moussa and G. A. Dakroury, *J. Sustain. Metall.*, 2022, **8**, 715–731.
101 T. Qiu, J.-G. Yang, X.-J. Bai and Y.-L. Wang, *RSC Adv.*, 2019, **9**, 12737–12746.
102 S. Kumar, Bhawna, A. Gupta, R. Kumar, A. Bharti, A. Kumar and V. Kumar, *J. Phys. Chem. C*, 2023, **127**, 7095–7106.
103 C. Ding, J. Guo, W. Gan, P. Chen, Z. Li, Z. Yin, S. Qi, S. Deng, M. Zhang and Z. Sun, *Sep. Purif. Technol.*, 2022, **297**, 121480.
104 M. V. Kangralkar, V. A. Kangralkar and J. Manjanna, *Environ. Nanotechnol. Monit. Manag.*, 2021, **15**, 100417.
105 A. S. Eltaweil, H. Ali Mohamed, E. M. Abd El-Monaem and G. M. El-Subruiti, *Adv. Powder Technol.*, 2020, **31**, 1253–1263.
106 M. Danish and M. Muneer, *J. Phys. Chem. Solids*, 2021, **149**, 109785.
107 M. Sarkhosh, M. Sadani, M. Abtahi, S. M. Mohseni, A. Sheikhmohammadi, H. Azarpira, A. A. Najafpoor, Z. Atafar, S. Rezaei, R. Alli and A. Bay, *J. Hazard. Mater.*, 2019, **377**, 418–426.
108 P. A. Ajibade and A. E. Oluwalana, *Nanomaterials*, 2021, **11**, 2000.
109 M. Ganguly, J. Jana, A. Pal and T. Pal, *RSC Adv.*, 2016, **6**, 17683–17703.
110 S. Ramasundaram, M. G. Seid, J. W. Choe, E.-J. Kim, Y. C. Chung, K. Cho, C. Lee and S. W. Hong, *Chem. Eng. J.*, 2016, **306**, 344–351.
111 P. Sharma, M. Sahu, M. Ganguly and A. Doi, *Sci. Rep.*, 2025, **15**, 19676.
112 M. Ganguly, A. Pal, Y. Negishi and T. Pal, *Langmuir*, 2013, **29**, 2033–2043.
113 V. K. Vidhu and D. Philip, *Micron*, 2014, **56**, 54–62.
114 G. A. Otunola, A. J. Afolayan, E. O. Ajayi and S. W. Odeyemi, *Pharmacogn. Mag.*, 2017, **13**, S201–s208.
115 P. Sharma, M. Ganguly and A. Doi, *Nanoscale Adv.*, 2024, **6**, 3476–3493.
116 K. Chaudhary, M. Aadil, S. Zulfiqar, S. Ullah, S. Haider, P. O. Agboola, M. F. Warsi and I. Shakir, *Fullerenes, Nanotub. Carbon Nanostruct.*, 2021, **29**, 915–928.
117 S. Guiza, H. Hajji and M. Bagane, *C. R. Chim.*, 2019, **22**, 161–168.
118 H. Chaudhary, K. Chaudhary, S. Zulfiqar, M. S. Saif, I. A. Alsafari, I. Shakir, P. O. Agboola, M. Safdar and M. F. Warsi, *Ceram. Int.*, 2021, **47**, 32521–32533.
119 L. El Gaini, *Desalination Water Treat.*, 2024, **320**, 100798.
120 H. Song, S. Luo, H. Huang, B. Deng and J. Ye, *ACS Energy Lett.*, 2022, **7**, 1043–1065.

121 B. Chandran, J.-K. Oh, S.-W. Lee, D.-Y. Um, S.-U. Kim, V. Veeramuthu, J.-S. Park, S. Han, C.-R. Lee and Y.-H. Ra, *Nano-Micro Lett.*, 2024, **16**, 244.
122 A. Aswin and A. R. Jeice, *Int. J. Adv. Sci. Eng.*, 2024, **10**, 3489–3494.
123 W. Li, S. Zhao, B. Qi, Y. Du, X. Wang and M. Huo, *Appl. Catal., B*, 2009, **92**, 333–340.
124 R. Jasrotia, Suman, A. Verma, R. Verma, J. Ahmed, S. K. Godara, G. Kumar, A. Mehtab, T. Ahmad and S. Kalia, *J. Water Proc. Eng.*, 2022, **48**, 102865.
125 K. Jhansi and P. Swaminathan, *J. Electron. Mater.*, 2025, **54**, 485–498.
126 D.-E. Lee, S. Moru, W.-K. Jo and S. Tonda, *Sep. Purif. Technol.*, 2025, **352**, 128261.
127 R. Rajan, S. Ahmed, N. Sharma, N. Kumar, A. Debas and K. Matsumura, *Mater. Adv.*, 2021, **2**, 1139–1176.
128 D. A. Gkika, A. K. Tolkou, I. A. Katsoyiannis and G. Z. Kyzas, *Sep. Purif. Technol.*, 2025, **368**, 132996.
129 Y. Trivedi, M. Sharma, R. K. Mishra, A. Sharma, J. Joshi, A. B. Gupta, B. Achintya, K. Shah and A. K. Vuppaladadiyamd, *Desalination*, 2025, **600**, 118509.
130 S. Satyam and S. Patra, *Heliyon*, 2024, **10**, e29573.
131 H. A. Elbadawy, A. F. Elhusseiny, S. M. Hussein and W. A. Sadik, *Sci. Rep.*, 2023, **13**, 2302.
132 Y. S. Jara, T. T. Mekiso and A. P. Washe, *Sci. Rep.*, 2024, **14**, 6997.
133 D. Gola, A. kriti, N. Bhatt, M. Bajpai, A. Singh, A. Arya, N. Chauhan, S. K. Srivastava, P. K. Tyagi and Y. Agrawal, *Curr. Res. Green Sustainable Chem.*, 2021, **4**, 100132.
134 S. Anjum, A. Rashid, F. Bashir, M. Pervaiz and R. Zia, *Mater. Today: Proc.*, 2015, **2**, 5559–5567.
135 J. Zhou, Z. You, W. Xu, Z. Su, Y. Qiu, L. Gao, C. Yin and L. Lan, *Sci. Rep.*, 2019, **9**, 5470.
136 X. Li, Y. Chen, Y. Tao, L. Shen, Z. Xu, Z. Bian and H. Li, *Chem Catal.*, 2022, **2**, 1315–1345.
137 M. F. Sanakousar, C. C. Vidyasagar, V. M. Jiménez-Pérez, B. K. Jayanna, Mounesh, A. H. Shridhar and K. Prakash, *J. Hazard. Mater. Adv.*, 2021, **2**, 100004.
138 B. Petrovic, M. Gorbounov and S. Masoudi Soltani, *Microporous Mesoporous Mater.*, 2021, **312**, 110751.
139 Z. Raji, A. Karim, A. Karam and S. Khalloufi, *Waste*, 2023, **1**, 775–805.
140 L. Koopal, W. Tan and M. Avena, *Colloids Surf., A*, 2019, **577**, 709–722.
141 A. R. Abbasi, M. Karimi and K. Daasbjerg, *Ultrason. Sonochem.*, 2017, **37**, 182–191.
142 A. Abdel-Aziz, N. Mohamed, R. M. El-taweel, S. Husien, Y.-T. Hung, L. A. Said, I. S. Fahim and A. G. Radwan, *Mater. Res. Express*, 2024, **11**, 065801.
143 X. Li, L. Zheng, L. Huang, O. Zheng, L. Zhenyu, L. Guo, B. Qiu and G. Chen, *J. Appl. Polym. Sci.*, 2013, **129**, 2857–2864.
144 R. Khani, B. Roostaei, G. Bagherzade and M. Moudi, *J. Mol. Liq.*, 2018, **255**, 541–549.
145 S. K. Shukla, S. Pandey, S. Saha, H. R. Singh, P. K. Mishra, S. Kumar and S. K. Jha, *J. Environ. Chem. Eng.*, 2021, **9**, 105847.
146 A. R. Abbasi, M. Rizvandi, A. Azadbakht and S. Rostamnia, *J. Colloid Interface Sci.*, 2016, **471**, 112–117.
147 A. R. Abbasi, M. Yousefshahi and A. Azadbakht, *Colloids Surf., A*, 2016, **498**, 58–65.
148 J. W. Steed, D. R. Turner and K. J. Wallace, *Core Concepts in Supramolecular Chemistry and Nanochemistry*, John Wiley & Sons, 2007.
149 D. B. Smithrud, E. M. Sanford, I. Chao, S. B. Ferguson, D. R. Carcanague, J. D. Evanseck, K. N. Houk and F. Diederich, *Pure Appl. Chem.*, 1990, **62**, 2227–2236.
150 H. Li, M. Eddaoudi, M. O'Keeffe and O. M. Yaghi, *Nature*, 1999, **402**, 276–279.
151 J. L. C. Rowsell and O. M. Yaghi, *Microporous Mesoporous Mater.*, 2004, **73**, 3–14.
152 G. O. El-Sayed, *Desalination*, 2011, **272**, 225–232.
153 Y. S. Ho and G. McKay, *Water Res.*, 2000, **34**, 735–742.
154 E. Eren, O. Cubuk, H. Ciftci, B. Eren and B. Caglar, *Desalination*, 2010, **252**, 88–96.
155 R. Palanivel and P. Koshy Mathews, *J. Cent. S. Univ.*, 2012, **19**, 1–8.
156 H. Liu, A. Robert and V. Luu-The, *J. Steroid Biochem. Mol. Biol.*, 2005, **94**, 173–179.
157 D. Vildozo, C. Ferronato, M. Sleiman and J.-M. Chovelon, *Appl. Catal., B*, 2010, **94**, 303–310.
158 R. Khani, S. Sobhani and M. H. Beyki, *J. Colloid Interface Sci.*, 2016, **466**, 198–205.
159 R. Naveenkumar and G. Baskar, *Bioresour. Technol.*, 2020, **315**, 123852.
160 Y. S. Ho and G. McKay, *Process Biochem.*, 1999, **34**, 451–465.
161 H. Freundlich, *Z. Phys. Chem.*, 1907, **57**, 385–470.
162 I. Langmuir, *J. Am. Chem. Soc.*, 1918, **40**, 1361–1403.
163 I. Rossetti, N. Pernicone, F. Ferrero and L. Forni, *Ind. Eng. Chem. Res.*, 2006, **45**, 4150–4155.
164 T. Bian, A. Gardin, J. Gemen, L. Houben, C. Perego, B. Lee, N. Elad, Z. Chu, G. M. Pavan and R. Klajn, *Nat. Chem.*, 2021, **13**, 940–949.
165 H.-X. Zhou and X. Pang, *Chem. Rev.*, 2018, **118**, 1691–1741.
166 M. Yang, Y. Zhao, H. Yan, Z. Wang, C. Xu, C. Zhang, E. Bilotti, J. Li and Z.-M. Dang, *Energy Environ. Sci.*, 2024, **17**, 7627–7648.
167 T. Chen, M. Li and J. Liu, *Cryst. Growth Des.*, 2018, **18**, 2765–2783.
168 C. R. Martinez and B. L. Iverson, *Chem. Sci.*, 2012, **3**, 2191–2201.
169 A. Abdel-Aziz, N. Mohamed, R. M. El-taweel, S. Husien, I. S. Fahim, L. A. Said and A. G. Radwan, *Results Eng.*, 2023, **20**, 101420.
170 Z. Wang, C. Chen, H. Liu, D. Hrynshpan, T. Savitskaya, J. Chen and J. Chen, *Sci. Total Environ.*, 2020, **708**, 135063.
171 N. Ayawei, A. N. Ebelegi and D. Wankasi, *J. Chem.*, 2017, **2017**, 3039817.
172 H. Alkhaldi, S. Alharthi, S. Alharthi, H. A. AlGhamdi, Y. M. AlZahrani, S. A. Mahmoud, L. G. Amin, N. H. Al-Shaalan, W. E. Boraie, M. S. Attia, S. A. Al-Gahtany, N. Aldaleeli, M. M. Ghobashy, A. I. Sharshir, M. Madani, R. Darwesh and S. F. Abaza, *RSC Adv.*, 2024, **14**, 35104.

173 N. R. Bhalodia and V. J. Shukla, *J. Adv. Pharm. Technol. Res.*, 2011, **2**, 104–109.
174 Q. Liu, P. Chen, Z. Xu, M. Chen, Y. Ding, K. Yue and J. Xu, *Sens. Actuators, B*, 2017, **251**, 339–348.
175 S. Singh, N. A. Khan, R. Ramadan, N. Shehata, D. Kapoor, D. S. Dhanjal, N. Sivaram, J. Singh, D. Barceló and P. C. Ramamurthy, *Desalination Water Treat.*, 2024, 100201.
176 A. Anchani, A. Abishini and T. Ashokkumar, *Discov. Biotechnol.*, 2024, **1**, 4.
177 V. Kumar, A. Barala and V. K. Goel, *Indian J. Pure Appl. Phys.*, 2023, **61**, 903–905.
178 A. Marubini, R. Mhlarhi and J. N. Edokpayi, *Sci. Afr.*, 2025, **28**, e02701.
179 M. U. Rehman, M. B. Taj and S. A. C. Carabineiro, *Chemosphere*, 2023, **338**, 139477.
180 A. S. Al-Wasidi, E. A. Abdelrahman, K. u. Rehman, F. A. Saad and A. M. Munshi, *Sci. Rep.*, 2024, **14**, 29599.
181 S. Aroob, S. A. C. Carabineiro, M. B. Taj, I. Bibi, A. Raheel, T. Javed, R. Yahya, W. Alelwani, F. Verpoort, K. Kamwilaisak, S. Al-Farraj and M. Sillanpää, *Catalysts*, 2023, **13**, 502.
182 M. A. Al-Ajji and M. A. Al-Ghouti, *J. Water Proc. Eng.*, 2021, **44**, 102354.
183 G. Schmid, *Chem. Rev.*, 1992, **92**, 1709–1727.
184 M.-C. Daniel and D. Astruc, *Chem. Rev.*, 2004, **104**, 293–346.